Advances in Magnetics

Modern Microwave Ferrites

Vincent G. Harris, *Fellow, IEEE*

Center for Microwave Magnetic Materials and Integrated Circuits and Department of Electrical and Computer Engineering, Northeastern University, Boston, MA 02115-5000 USA

Microwave ferrites are ubiquitous in systems that send, receive, and manipulate electromagnetic signals across very high frequency to quasi-optical frequency bands. In this paper, modern microwave ferrites are reviewed including spinel, garnet, and hexaferrite systems as thin and thick films, powders and compacts, and metamaterials. Their fundamental properties and utility are examined in the context of high frequency applications ranging from the VHF to millimeter-wave bands. Perspective and outlook of advances in theory, processing, and devices occurring in the science and engineering communities since the year 2000 are presented and discussed.

Index Terms—**Circulator, density functional theory, ferrite, garnet, hexaferrite, liquid phase epitaxy, microstrip filter, microstrip phase shifter, molecular field theory, negative index metamaterials, pulsed laser deposition, screen printing, spinel, spin spray plating.**

I. Introduction and Historical Development

MICROWAVE magnetic materials operate either near the natural resonance, as absorbers or electromagnetic interference shielding materials, or above or below resonances as low-loss, high permeable materials in devices such as circulators, isolators, phase shifters, filters, inductor cores, etc.

The focus of this review is principally in the area of off resonance materials and their applications. As the operational frequency of these materials increases, the requirement for low-loss properties also increases, thus necessitating insulating magnetic materials.

Ideal materials possess high magnetization, high permeability, high permitivity, high electrical resistivity, and low electronic and magnetic losses. Insulating magnetic materials that fit this criteria include ferrites and related magnetic oxides.

Ferrite materials have been known to ancient cultures for many centuries. The first known reference to ferrite materials dates to an ancient text by Guan Zhong (725-654 BCE) who described lodestone, naturally occurring minerals rich in Fe_3O_4, as "ci shi" or "loving stone" [1]. A similar reference to lodestone was made by the Greek philosopher Thales of Miletus [2] in the 6th century BCE [3]. Fragments of lodestone suspended in a fluid, typically water, naturally orient towards a magnetic pole thus enabling the development of the first magnetic compasses [4]. The first suspended magnetic needle compass was described by Shen Kuo in CE 1088 [5]. Although lodestone found great utility in compasses for both terrestrial and nautical navigation, it was not until c. 1936 that modern ferrites were studied for their magnetic, structure, and electronic properties for use as high induction cores in power generation, conditioning, and conversion applications.

Manuscript received September 18, 2011; accepted November 02, 2011. Date of publication December 21, 2011; date of current version March 02, 2012. Corresponding author: V. G. Harris (e-mail: harris@ece.neu.edu).

Color versions of one or more of the figures in this paper are available online at http://ieeexplore.ieee.org.

Digital Object Identifier 10.1109/TMAG.2011.2180732

The value of ferrites as materials for ultrahigh frequency applications was not realized until c. 1940 when ferrites were systematically studied by Snoek *et al.* [6], [7] for applications in devices that send, receive, and manipulate electromagnetic signals at radio-frequency (rf), microwave, and millimeter-wave frequencies.

Ferrite materials are unique because they are one of a few classes of insulating magnetic oxides that possess moderate values of magnetization, high permeability, moderate to high permittivity, and low-losses at frequencies from dc to sub-millimeter wavelengths. These properties afford them great value in high frequency devices that require strong coupling to electromagnetic signals while experiencing low losses. Additionally, due to their intrinsic magnetism, these materials also provide non-reciprocal behavior that is essential for many device applications in radar and communications systems as isolators, circulators, etc. These properties and applications will be discussed in detail later in this review.

Popular engineering ferrites principally exist as cubic and hexagonal structures having close-packed oxygen lattices. Cubic ferrites include garnets and spinels, whereas the hexaferrites can exist in several structural variants, e.g., M, Y, Z, U, W, in which the metal and oxygen stoichiometry vary [34], [39]. Due to their highly symmetric structures and low intrinsic magnetocrystalline anisotropy energy, cubic ferrites tend to have low magnetic anisotropy fields, while hexaferrites may possess extremely high magnetic anisotropy fields. As will be discussed in greater detail, the ferromagnetic resonance (FMR) frequency shifts with changes in magnetic anisotropy field(s), together with demagnetizing field, magnetization and applied magnetic fields (also known as bias fields), leading to the application of cubic spinels at UHF, rf and microwave frequencies and hexaferrites at microwave, mm-wave, sub-mm wave, and quasi-optical frequencies.

In this review, we present recent advances in ferrite materials of various forms. For example, we will discuss the latest trends in processing, composition, theory, and the utility of ferrite films, crystals, compacts, metamaterials, and other unique het-

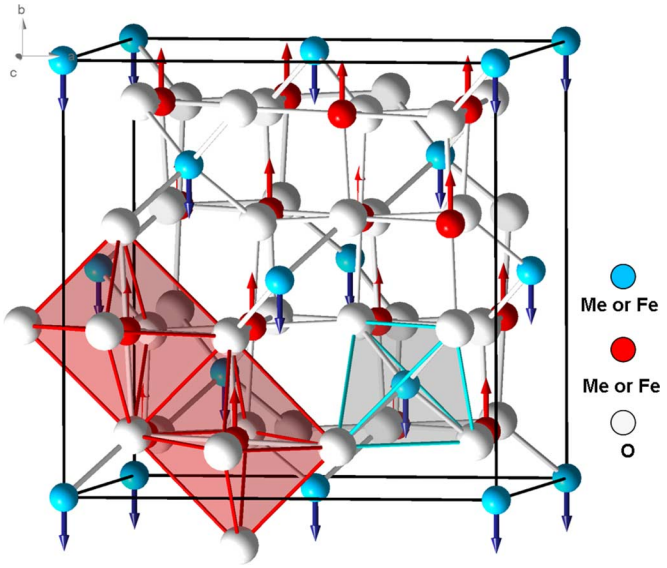

Fig. 1. Schematic representation of spinel ferrite structure. (Adapted from [87].)

erostructures. We will focus our review towards high frequency properties and applications ranging from ~0.01–100 GHz.

II. Structure and Chemistry of Ferrites

As previously mentioned, ferrites exist principally as garnet, spinel, and hexaferrite structures. In this section, we present a discussion of each material system in terms of their crystal structure, chemistry, and magnetic and microwave properties. This discussion will be brief and is intended to provide the reader a broad overview of the fundamental physical and chemical principles required to better understand the functional properties and utility of ferrites.

The ferrite structure, be it spinel, garnet, or hexaferrite, has as its structural backbone a close packed structure of oxygen anions. Metallic cations, magnetic and nonmagnetic, and typically divalent and trivalent, reside on the interstices of the close packed oxygen lattice in some cases filling all available sites, while in others preferentially filling select sites.

A. Spinels

The spinel structure, space group $Fd3m$, is typically expressed in the form $[\mathrm{A}]\{\mathrm{B}\}_2\mathrm{O}_4$ (where [ ] indicates divalent cations occupying four-fold tetrahedra lattice sites and { } indicates trivalent cations occupying six-fold octahedra lattice sites). $[\mathrm{A}]\{\mathrm{B}\}_2\mathrm{O}_4$ is a single formula unit that constitutes 1/8 of the spinel unit cell (see Fig. 1). Cations have either four-fold or six-fold coordination forming tetrahedra (A) and octahedra (B) sublattices that are arranged in a close packed arrangement with respect to each other. A cations reside on 8 of 64 available tetrahedral sites whereas B cations reside on 16 of 32 available octahedral sites. Oxygen anions form a close packed structure and contribute 32 ions that electrically balance the unit cell.

The most popular and abundant of the magnetic spinels is magnetite, $\mathrm{Fe_3O_4}$, or $[\mathrm{Fe^{III}}]\{\mathrm{Fe^{III}Fe^{II}}\}_2\mathrm{O}_4$, which has 8 trivalent Fe ions on the A sublattice and a mix of divalent (8) and trivalent (8) ions on the B sublattice. As we will discuss, this structure and cation distribution is referred to as an *inverted* spinel. Briefly, the γ form of $\mathrm{Fe_2O_3}$ is also a spinel in which vacancies form preferentially on the B sublattice in the form of $[\mathrm{Fe^{III}}]\{\mathrm{Fe^{III}_{1.7}X_{0.3}}\}\mathrm{O}_4$ where X denotes vacancies.

Magnetism in these structures arises from superexchange interaction [8]–[11]. In the ground state superexchange is a negative exchange interaction that results in the antialignment of cation spins (i.e., ferrimagnetic). This, together with the dilution introduced by the oxygen lattice, is the principle reason that ferrite magnetization is significantly reduced in comparison to the magnetism of most $3d$ metallic alloys, e.g., Fe, Co, Ni, etc., which are governed by direct exchange in which the spins are aligned parallel (i.e., ferromagnetic). It is also the reason that it is difficult to increase the magnetization of ferrite materials being that there is little flexibility in creating long-range networks of collinear spins of high moment.

Because the A-site and B-site spins are antiparallel to one another, a strategy to increase the net magnetization (M) is to create an imbalance between sublattice magnetizations. This is typically done by substituting nonmagnetic cations for magnetic ions. A popular example is the substitution of $\mathrm{Zn^{II}}$ for A-site $\mathrm{Fe^{III}}$ cations. As one increases the fraction of $\mathrm{Zn^{II}}$ on the A-sublattice the net magnetization increases. However, this increase occurs at the expense of the strength of the AB exchange energy. This strategy works to a point and then the spins on the A and B sublattices *cant* (or twist) due to the reduction in the exchange constant, J_{AB}, leading to a reduction in magnetization. For this reason, cation substitutions must be carefully chosen to maximize M while concomitantly maintaining a strong J_{AB}.

Weakened exchange leading to spin canting is also prominent in most ferrite particle systems when the effective diameter approaches nanoscale. Surface spin disorder has been attributed by Kodama *et al.*, [12] to account for the inability to saturate nanoparticle ferrites in fields as high as 160 kOe. Surface spin disorder is determined by the surface crystallography and the breaking of more A-B than B-B exchange bonds in forming trigonal (111) surfaces. This is equivalent to the conditions for forming Yafet-Kittel triangular spin structures [13] in bulk ferrites with non-magnetic substituents (e.g., Zn in NiZn and MnZn ferrites) which is amplified where surface symmetry breaking results in noncompensated spins in the near surface region [14]. McHenry *et al.*, have proposed that surface spin canting originates in ferrite nanoparticles from preferred termination of crystallographic planes with (111) planes being more prevalent at smaller nanoparticle sizes [14], [15]. Such preferred termination lead naturally towards a nonequilibrium ratio of octahedral to tetrahedral site distribution and an eventual weakening of net A-B exchange integrals favoring triangular spin structures as described by Yafet and Kittel. The literature is replete with reports of nanoparticle ferrite studies and it is not the intention of this article to review this literature. The reader is directed to a review of magnetic nanoparticles by Willard *et al.* [16], and references contained within.

Spinels can be classified as *normal*, *inverse*, or *mixed*. The *normal* spinel has only divalent cations residing on the 8 A sites with trivalent ions filling the 16 B sites. An example of a *normal* ferrite is the aforementioned Zn spinel ferrite ($[\mathrm{Zn^{II}}]\{\mathrm{Fe^{III}}\}_2\mathrm{O}_4$) where divalent Zn fill A-sites and trivalent Fe the B sites. Alternatively, when divalent ions fill 8 of the 16 B sites with trivalent ions occupying the remaining A and

TABLE I
SPINEL CATION DISTRIBUTION, MAGNETISM, CURIE TEMPERATURE, MICROWAVE PROPERTIES AND RESISTIVITY

Ferrite Composition	Tetrahedral ion distribution[17)]	Octahedral ion distribution[17)]	$4\pi M_s$ (G)[18)]	T_c (K)[19)]	ΔH (Oe)	g (at X-band)[20)]	ρ (Ω-cm)
Fe_3O_4	Fe^{III}	$Fe^{II}+Fe^{III}$	6000	858		2.017	10^{-2}
$MnFe_2O_4$	$Fe_{0.2}{}^{III}+Mn_{0.8}{}^{II}$	$Mn_{0.2}{}^{II}+Fe_{1.8}{}^{III}$	4800	577	600	2.004+/- 0.002	10^{4} [21)]
$CoFe_2O_4$	Fe^{III}	$Co^{II}+Fe^{III}$	5300	793		2.27	10^{4}
$NiFe_2O_4$[e)]	Fe^{III}	$Ni^{II}+Fe^{III}$	3000	860	350	2.3	10^{9}
$CuFe_2O_4$	Fe^{III}	$Cu^{II}+Fe^{III}$	1700	728		2.05	
$MgFe_2O_4$[e)]	Fe^{III}	$Mg^{II}+Fe^{III}$	1500	710	900	2.06	10^{6}
$Li_{0.5}Fe_{2.5}O_4$	Fe^{III}	$Li_{0.5}{}^{I}+Fe_{1.5}{}^{III}$	3900	943	14 (SX)	2.08 (SX)	10^{-2}

Unless denoted, sample is a polycrystalline compact

SX: single crystal

a) [17] Smit, J. and Wijn, H. P. J., (1959), *Ferrites*, New York, Wiley, New York, p. 149.

b) [18] Smit, J. and Wijn, H. P. J., (1959), *Ferrites*, New York, Wiley, New York, p. 157.

c) [19] Smit, J. and Wijn, H. P. J., (1959), *Ferrites*, New York, Wiley, New York, p. 157.

d) [20] Smit, J. and Wijn, H. P. J., (1959), *Ferrites*, New York, Wiley, New York, p. 174.

e) [21] von Aulock, W.H., (1965), *Handbook of Microwave Ferrite Materials*, (New York) Academic Press.

B sites, an *inverse* spinel results. An example of an inverse spinel is Ni-ferrite $([Fe^{III}]\{Ni^{II}_{0.5}Fe^{III}_{0.5}\}_2O_4)$. As we will see, these designations are not strictly adhered to since the nature of ferrite processing is often of a nonequilibrium nature and leads to a degree of cation disorder in which cations redistribute from their preferred sites.

Finally, the *mixed* spinel has different ions of mixed valence occupying both A and B sublattices. Because each species of ion has thermodynamically preferred lattice distributions based predominantly on cation ionic radius, electrostatic energy, and electronic configuration, this class of ferrite commonly results from nonequilibrium processing such as those that involve vapor quenching (e.g., pulsed laser deposition, sputter deposition) and high kinetic energy transfer (e.g., ball milling), among other techniques. Cation species that exist naturally in a multiple of valence states are more susceptible to this type structure. For example, Mn ions with common valences of 2, 3, 4, 6, and 7, and of comparable size to Fe ions, allow for such a distribution as $[Mn^{II,III}_{1-\delta}Fe^{II,III}_{\delta}]\{Mn^{II,III}_{\delta}Fe^{II,III}_{2-\delta}\}O_4$ to exist (where δ represents the cation inversion parameter). The tendency to stabilize defects in such structures adds yet another degree of complexity. As one might imagine, determining such a structure with robust measurement statistics represents a significant challenge to the experimentalist.

Table I presents some common spinel ferrite materials with their preferred cation distributions, magnetization, Curie temperatures, FMR linewidths, and related properties. It is important to realize, as stated earlier, that nonequilibrium processing leads to deviations from the listed cation distributions.

B. Garnets

When considering cubic ferrites, garnets hold an important position in that they have superior insulating properties, and as such, are choice materials for applications in which the minimization of conduction losses is an important consideration. In this review, we limit our discussion to select compositions that have particular value at UHF, rf and microwave frequencies with an emphasis on the industrially important yttrium iron garnet (YIG) (see Fig. 2). Table II presents magnetic, electronic, and microwave properties of selected garnets.

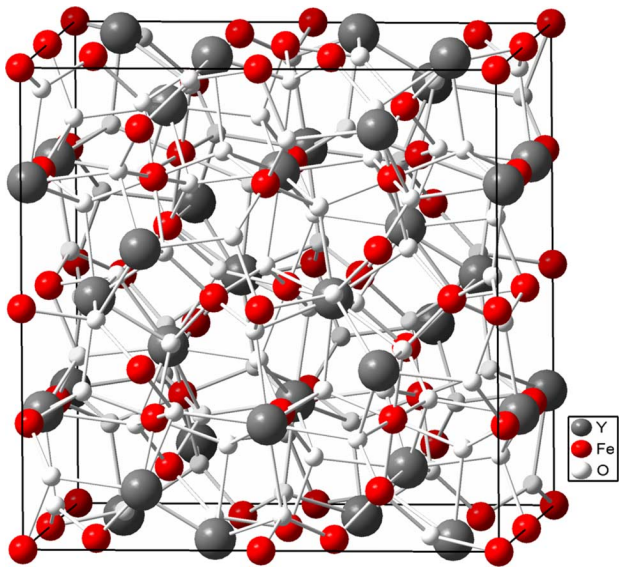

Fig. 2. Schematic representation of garnet (YIG) structure. (Adapted from [87].)

Mineral garnets are based on a Si-oxide structure with additions of Mn and Al (i.e., $Mn_3Al_2Si_3O_{12}$). Yoder and Keith [22] were first to show in 1951 that substitutions of Y^{III} and Al^{III} for Mn^{II} and Si^{IV} allow for the stabilization of a Si-free structure, $Y_2Al_5O_{12}$. This led Bertaut and Forrat [23] in 1956

TABLE II
PROPERTIES OF MAGNETIC GARNETS (MICROWAVE PROPERTIES WERE MEASURED AT X-BAND)

Material	$4\pi M_s$ (G)	T_c (K)	ΔH (Oe)	g	ρ (Ω-cm)	Comment
$Y_3Fe_5O_{12}$	1750	550-560	15 0.1 (SX)	2.00	$1x10^{10}$	Ref. 26
$Y_3Fe_{4.67}Al_{0.33}O_{12}$	1200	500	44	2.02		Ref. 27
$Y_3Fe_{4.5}Ga_{0.5}O_{12}$	1000	490	50	2.01	$1x10^{8}$	Ref. 27
$Y_3Fe_{4.5}Cr_{0.5}O_{12}$	1800	505	140	2.15		Ref. 27
$Y_2GdFe_5O_{12}$	1200	560	110	2.00		Refs. 27 and 28
$Y_2NdFe_5O_{12}$	1930	551	2 (SX)		$5x10^{7}$	Ref. 29
$Y_2SmFe_5O_{12}$	1710	550-555	100 (SX)	2.00		Ref. 29

Unless denoted, sample is a polycrystalline compact

SX: single crystal

[26] G.R. Harrison, L.R. Hodges, Jr., *J. Am. Ceram. Soc.*, vol. 44, p. 214, 1961.

[27] A. Vassiliev, J. Nicolas, and M. Hildebrant, *C.R. Acad. Sci.*, vol. 252, p. 2529, 1961.

[28] G. Goldring, M. Schieber, and Z. Vager, *J. Appl. Phys.*, vol. 31, p. 2057, 1960.

[29] W.H. von Aulock, *Handbook of Microwave Ferrite Materials*, New York, Academic Press, 1965.

to report the structure and magnetic properties of $Y_3Fe_5O_{12}$, YIG; space group $Ia3d$. Fig. 2 is a representation of the YIG unit cell. YIG has a high Verdet constant which provides a large magneto-optical response, high Q factor at microwave frequencies, low absorption in the infrared (up to 600 nm), and small FMR linewidth [24]. YIG is used in rf, microwave, optical, and magneto-optical applications, for example as microwave filters. It also finds utility in solid-state lasers, Faraday rotators, and in nonlinear optical applications.

In the YIG structure, trivalent Fe ions occupy two octahedral and three tetrahedral sites. The yttrium ions are too large to occupy the tetrahedral and/or octahedral sites and too small to substitute for the oxygen anion. They instead occupy sites that are irregularly surrounded by 8 oxygen ions in a distorted cube. In the garnet unit cell all possible cation positions are filled leading to uncommon chemical and structural stability as well as high insulating properties.

The Fe ions on the A and B sites are coupled ferrimagnetically by superexchange as in the spinel systems. The net moment derives from the excess Fe^{III} on tetrahedral sites. The Curie temperature also derives from superexchange and is nearly the same for all garnets ~560 K [25]. However, the saturation magnetization and the magnetic anisotropy field are rather low, $4\pi M_s = 1740$ G and $H_a = 40$ Oe, respectively, compared with other ferrite systems resulting in a low FMR frequency. For these reasons, YIG is usually biased by permanent magnets for microwave devices applications. Notwithstanding the need for bias magnets, YIG is a choice material for many applications at frequencies up to and including X-band, above which the bias magnet size, weight and cost become prohibitive.

At higher frequencies, ferrites with substantially higher magnetization and magnetic anisotropy are required. For this we turn to hexaferrites.

C. Hexaferrites

In contrast to the spinel and garnet ferrites, the hexaferrites have hexagonal crystal symmetry leading to high magnetocrystalline anisotropy energies and magnetic anisotropy fields (H_A) and subsequently high FMR frequencies. Among the most popular of the microwave hexaferrites are those derived from the Ba M-type (or BaM) hexaferrite, $BaFe_{12}O_{19}$ (see Fig. 3). BaM has the magnetoplumbite structure, space group Pb_3/mmc, and consists of 10 oxygen layers in which four successive layers each containing four oxygen anions are followed by a fifth layer containing three anions and a Ba cation. The structure is constructed of spinel (S) blocks containing two oxygen layers separated by an R block containing the Ba ion. Every other S and R block is rotated 180° with respect to the other and is denoted

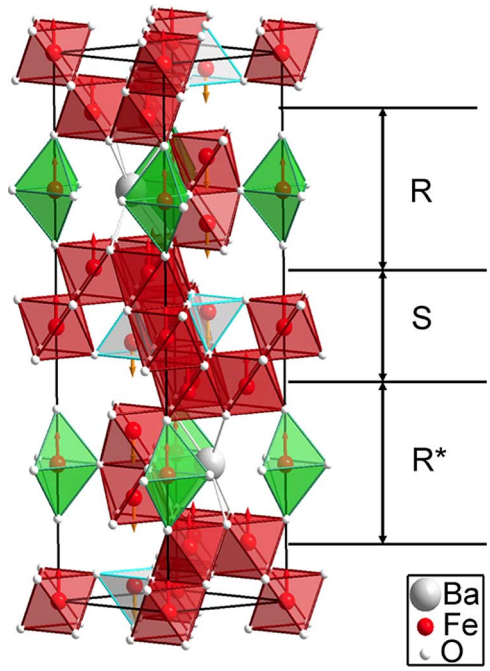

Fig. 3. Schematic representation of magnetoplumbite structure (BaM). (Adapted from [87].)

TABLE III
HEXAFERRITE STRUCTURE, MAGNETISM, CURIE TEMPERATURE, AND ANISOTROPY FIELDS [39]

Ferrite	Designation, structure	$4\pi M_s$ (G)	T_C (K)	H^A_θ (Oe)	H^A_φ (Oe)[40]
$BaFe_{12}O_{19}$	M: RSR*S*	4770	725	17,000	
$BaFe_{18}O_{27}$	Fe_2W: RSSR*S*S*	3940	728	19,000	
$BaZnFe_{17}O_{27}$	FeZnW: RSSR*S*S*	4770	703	12,500	
$BaMnZnFe_{16}O_{27}$	Fe(MnZn)W: RSSR*S*S*	4650		10,200	
$BaNi_2Fe_{16}O_{27}$	Ni_2W: RSSR*S*S*	4145	793	12,700	
$Ba_2Mg_2Fe_{12}O_{22}$	Mg_2Y: RSR*S*TS*	1500	553	10,000	
$Ba_2Ni_2Fe_{12}O_{22}$	Ni_2Y: RSR*S*TS*	1600	663	14,000	
$Ba_2Zn_2Fe_{12}O_{22}$	Zn_2Y: RSR*S*TS*	2850	403	9,000	1
$Ba_2Co_2Fe_{12}O_{22}$	Co_2Y: RSR*S*TS*	2325	613	28,000	155
$Ba_3Co_2Fe_{24}O_{41}$	Co_2Z: RSTSR*S*T*S*	3390	683	13,000	16
$Ba_3Zn_2Fe_{24}O_{41}$	Zn_2Z: RSTSR*S*T*S*	3900	633		

Unless denoted, sample is a polycrystalline compact

[39] Smit, J. and Wijn, H. P. J., (1959), *Ferrites*, New York, Wiley, New York, 191, p. 204.

[40] Smit, J. and Wijn, H. P. J., (1959), *Ferrites*, New York, Wiley, New York, 191, p. 210.

as S^* and R^*, respectively. Trivalent Fe ions occupy tetrahedral and octahedral sites (derived from the spinel blocks) as well as one trigonal bypyramidal (TBP) site. The TBP site resides on the Ba-containing layer amidst the triagonal arrangement of oxygen anions [30].

There exist other hexaferrite structures designated as: Y, U, W, X, and Z, each having different structures and oxygen stoichiometry and markedly difference magnetic properties. For example, the Y-type structure, $\mathrm{Ba_2Me_2Fe_{12}O_{22}}$, consists of the stacking of S and T blocks were the T blocks can be thought of as R blocks in which the inner most atomic layer is repeated. Having defined the S, R, and T blocks, one can describe the W-type, $\mathrm{BaMe_2Fe_{16}O_{27}}$, as a stacking of $SSRS^*S^*R^*$, and the Z-type, $\mathrm{Ba_3Me_2Fe_{24}O_{41}}$, as R^*STSRS^*. The reader is directed to the literature to explore further types of hexaferrite structures [30]. The magnetization of the hexaferrites derives from superexchange interactions among the cation sublattices. The spin coupling and orientation of ferric ions in the S block mirrors those of the spinel ferrites and include two A and four B site ions. The ferric ion spin located in the R block TBP site is parallel the c-axis with its spin up orientation determined by the strength of the oxygen mediated superexchange and number and distance of near neighbor ferric ions.

Table III presents the stoichiometry of these compounds together with their room temperature saturation magnetization and anisotropy fields that demonstrate clearly the ability to tailor anisotropy and magnetization by cation substitution. Taken together, these parameters also determine the FMR frequency and hence operational bands.

We will next discuss the properties of M-type ferrites with the implication that materials processing and device refinement are transferable to other ferrite systems such as Y, W, U, and Z type ferrites.

The $\mathrm{Ba}M$ system is remarkably versatile in that substitution for the Fe cation can drastically reduce or increase $\mathrm{H_A}$, thus shifting the FMR frequency and the operating frequency of devices. For example, the substitution of Sc or In for Fe reduces $\mathrm{H_A}$ allowing for applications from X-, Ku-, K-, to Ka-bands [31]–[33]. While substitution of Al and Ga lead to increases in $\mathrm{H_A}$ and device operation at frequencies up to and including U-, E-, and W-bands [34]–[36]. In essence, the $\mathrm{Ba}M$ hexaferrite, and its substitutional systems, allow for device applications from 1 to >100 GHz.

The utility of M-type ferrites stems in part from the alignment of the easy magnetic direction along the crystallographic c-axis and the ability to process these materials with a high degree of crystal texture and preferential magnetic anisotropy. For example, the growth of $\mathrm{Ba}M$ films with the crystallographic c-axis aligned perpendicular to the film plane leads to perpendicular magnetic anisotropy: a requirement for conventional circulator and isolator devices and perpendicular magnetic storage media.

Unlike the M-type ferrites, Y- and Z-type ferrites have their magnetic easy axis aligned within the a-b or basal plane. Where the M-type hexaferrites can be saturated relatively easily by fields applied along the c-axis, the Y- and Z-type ferrites can be saturated by a small field aligned within the basal plane. This is of particular value for conventional phase shifter, delay lines, filter devices, and some antenna substrate applications.

In the hexaferrites, R and T blocks break crystal symmetry resulting in the hexagonal structure and large magnetocrystalline anisotropy energies common to these compounds. Also contributing to the magnetic anisotropy are dipolar interactions and single ion anisotropy. Remarkably, the magnetic anisotropy field in hexaferrites can reach several 10,000s Oe. Take for example $\mathrm{Ba}M$, where $\mathrm{H_A}$ is ~17,000 Oe, or ~1000–10,000 times greater than some cubic ferrites [30], [37]. The $\mathrm{H_A}$ places the zero field FMR frequency near 36 GHz. Thus, while an externally applied magnetic field is still necessary to saturate the ferrite during device operation, the magnitude of the applied field required to shift FMR to high frequencies is substantially reduced. As such, devices based upon this ferrite can operate at frequencies as high as Ku-band for below resonance operations and beyond Q-band for above resonance operations.

Textured polycrystalline hexaferrites can be produced with permanent magnet properties, such that they remain in a mag-

netized state in the absence of an externally applied magnetic field. In this condition, referred to as self-biased, the high internal bias field required for device operation at high frequencies is achieved without external magnets. Bias magnets hinder efforts to reduce the size and weight of devices, assemblies, and systems, such as transmit and receive modules in radar and communication systems. Further discussion of self-biased ferrite follows in Sections V-D and V-E.

In contrast to the hexaferrites mentioned so far, which are popular for high frequency low-loss applications, strontium-based hexaferrites are a permanent magnet that is characterized as having a saturation induction of 4650 G, high coercivity, ∼4000 Oe, and high remanence magnetization [37]. Strontium ferrite is a popular ceramic permanent magnet that has found great utility in many cost-effective commercial applications.

III. Ferrite Magnetism

A. Molecular Field Theory

An early theory of ferromagnetism was developed based on seminal studies performed by Weiss [41]. Weiss built on the then recent theory of Langevin who introduced the theory of paramagnetism [42]. Weiss' theory proposed the existence of long-range magnetic order in which a molecular field defines the interaction between spins. This theory successfully addressed many of the experimental observations of ferromagnetic behavior in metals at the time, including the temperature dependent behavior of magnetization and the existence of magnetic domains. However, it failed when applied to ferrites and other magnetic oxides that we now know are ferrimagnetic or antiferromagnetic. Néel put forward a molecular field theory as an expansion of the Curie-Weiss theory [11]. His theory introduced multiple molecular fields to describe coupled aligned and antialigned spin lattices to explain complex thermomagnetic behavior in ferrite and other magnetic oxide systems. Néel introduced to the magnetics community the concept of ferrimagnetic and antiferromagnetic interactions.

In considering the magnetic oxide systems discussed here, the exchange energy, J, between spins of neighboring metallic ions is negative resulting in the antiparallel alignment of spins as the lowest energy configuration. Since the distance between metal ions is too great to support direct exchange, such as that experienced in most magnetic metals, the exchange is mediated by the oxygen anion that resides between the two cations and is thus considered an indirect exchange, i.e., superexchange. Three factors principally affect the strength of the exchange, these include, the distance, direction, and angle of the cations with respect to the anion. While the direction and angle are defined by the relationship between Me-O-Me, the critical distance is that between Me-O not Me-Me, the later having little impact on J. All three factors determine the degree of orbital overlap between the extending 2p orbitals of oxygen and the 3d orbitals of the cations and hence the magnitude of J. By examining p- and d-orbital alignments one can readily conclude that larger Me-O-Me angles produce stronger negative exchange, while angles that approach 90° produce weak exchange. This is seen in the ferrite systems where, for example, in spinel ferrites the exchange J_{AB} corresponds to the largest A-O-B angle, $\sim 154°$, which is far larger than that of the B-O-B, J_{BB}, $\sim 125°$. The A-O-A correlation forms an angle less than 80° and the distance between A-O is comparatively larger, ~ 3.5 Å, leading to the smallest exchange, J_{AA}. J_{AA} is so comparatively small that many report this to be zero or ignore it altogether [17]. Magnetization results from an imbalance of spins on the ferrimagnetically coupled sublattices. As mentioned previously, one approach to increasing the net magnetization is to populate one sublattice preferential to the other with nonmagnetic cations while concomitantly maintaining a strong exchange energy, J, to minimize spin canting. Alternatively, one may populate one sublattice relative to the other with high spin moments. For a thorough treatment of molecular fields in ferrites, the reader is directed to a recent text by Dionne [43].

Although molecular field theory explain many aspects of ferrite behavior, they do not allow for determination of key intrinsic properties such as the exchange integral, energy gap, and magnetic ordering temperatures via a first principles self-consistent formalism.

Because magnetism in ferrites derives from an indirect interaction of valence electrons mediated by an anion, a self-consistent quantum theory of ferrite magnetism has remained elusive.

B. Density Functional Theory

Recent advances in density functional theory applied to oxide systems derive from basic observations in applying the Hubbard model.

The Hubbard model, introduced in 1963 [44], is based on the tight-binding approximation in which electrons are viewed as occupying standard orbitals "hopping" between atoms during conduction. The competition between the hopping integral and onsite repulsion explains the transition from conductor to insulator in many transition metal oxides including many ferrites.

Let us examine the prototypical case of Mn-ferrite in which basic mechanisms behind ferrimagnetic and insulating ground states are understood in the framework of Hubbard [45], [46].

As previously mentioned, the superexchange interaction between cations on A and B sites, J_{AB}, is negative. Since J_{AB} is negative and larger than the antiferromagnetic J_{BB} and J_{AA}, Mn ferrite has a ferrimagnetic ground state [47]. This has been confirmed by neutron diffraction experiments [48]. The insulating property of this material was confirmed by activation energy experiments by Lotgering [49].

In order to obtain accurate calculation of the exchange integrals and energy gap, values of the transfer integral (t), on-site Coulomb repulsion (U), and charge-transfer energy (D) are required. These cannot be ascertained in a self-consistent fashion using the Hubbard model or molecular field theories.

Current band theories fail when applied to magnetic transition-metal oxides due to the inaccuracy of the single electron approximation and the acute sensitivity to forms of exchange and correlation functionals. For example, application of Hartree-Fock (HF) [50], yields an antiferromagnetic exchange weaker than experimental values and larger band gaps. Alternatively, local spin-density approximation [51] (LSDA) tends to underestimate the band gap. Corrections to LSDA have been profered,

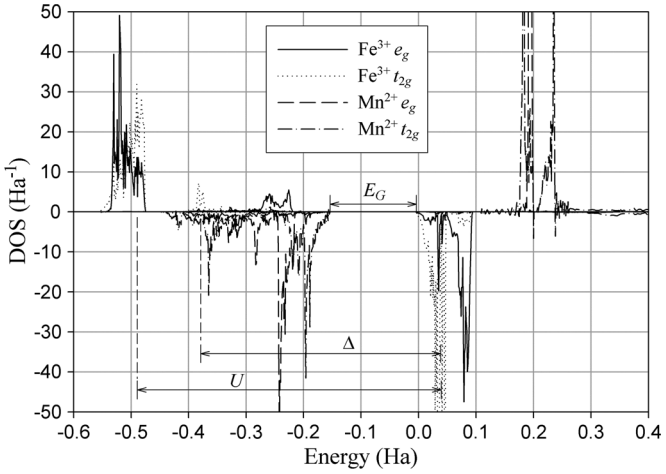

Fig. 4. Density of states, DOS, projected on sites and the d orbits of magnetic ions for the magnetic structure at a $w = 40\%$ calculated using an optimized basis set. (Adapted from [58]).

such as the self-interaction correction (SIC) [52], generalized gradient approximation [53], [54] (GGA), and LSDA1U [55]. These were designed to improve band gap calculations. However, in the case of LSDA1U, U is an *ad hoc* parameter, while the SIC and GGA have proven inadequate [56] for the case of magnetic oxides. The reason these calculations fail to predict the correct band gap and exchange is due to inaccurate predictions of U and t. Because HF underestimates t and overestimates U, it underestimates superexchange and overestimates band gap. Since LSDA overestimates t and underestimates U, overestimates superexchange and underestimates band gap. These failures are related to the choice of exchange-correlation functional to describe electron-electron interaction. Because of the need to compensate for such dependencies, a mixture of Fock exchange and LSDA, based on the linear interpolation of the adiabatic Kohn-Sham density functional [57], was recently shown to provide a path towards accurately predicting superexchange strength and band gap.

In 2002, Zuo and Vittoria [58] applied a mixture of Fock and Becke exchange to predict intrinsic magnetic and electronic properties of $\mathrm{MnFe_2O_4}$. J_{AB}, J_{BB}, E_G, U, and D as a function of w were calculated, where w was a weighting factor. They found that J_{AB} and J_{BB} agreed with experimental values, and that $\mathrm{MnFe_2O_4}$ was, calculated to be an insulator using a self-consistent approach.

In Fig. 4, Zuo and Vittoria show that U and Δ for $\mathrm{Fe^{III}}$ is dominated by the t_{2g} bands. (In [58], they also present a corresponding set of U and Δ values for the $\mathrm{Mn^{II}}$ ion.) E_G is simply the separation between the valence and conduction bands at the Fermi level. As stated by Zuo [58], overestimated electron-electron correlation in LSDA or GGA implies easier transfer of $3d$ electrons from one magnetic ion to another, which means a higher conductivity at finite temperature or a narrower band gap, which also means a lower potential barrier or a smaller U. In the DOS given by LSDA or GGA, if U of $\mathrm{Fe^{III}}$ was increased, the spin-down $\mathrm{Mn^{II}}$ d band and spin-down $\mathrm{Fe^{III}}$ d band would separate and the structure becomes insulating. Unfortunately, the underestimated electron-electron correlation yields the opposite

TABLE IV
COMPARISON BETWEEN THEORY AND EXPERIMENT

	J_{AB} (K)		J_{BB} (K)	
	normal	inverse	normal	inverse
Fock and Becke[h]	-15.3[a] -18.3[c]	-14.5[b] –21.4[d]	11.3[a] -4.4[c]	7.3[b] -12.0[d]
Experiment	-22.7[e], -19.1[f]		-3.070[f]	
HF	-4.7	-4.4	10.2	6.6
LSDA	---		---	
GGA	-464[g]		---	

a. Using optimized basis sets and evaluated at $w = 40\%$.
b. Using optimized basis sets and evaluated at $w = 50\%$.
c. Using the basis sets with expanded $3d$ wave functions and evaluated at $w = 30\%$.
d. Using the basis sets with expanded $3d$ wave functions and evaluated at $w = 40\%$.
e. [59] Heager, A.J. and Houston, T.W., (1964) *Phys. Rev.* 135, A661.
f. [60] Wegener, W., Scheerlinck, D., Legrand, E., and Hautecler, S., (1974), *Solid State Commun.* 15, 345.
g. [61] Singh, D.J., Gupta, M., and Gupta, R., (2002), *Phys. Rev.* B 65, 064432-1.
h. [58] Zuo, X., and Vittoria, C., (2002), *Phys. Rev.* B66, 184420.

result. Since the functional chosen by Zuo and Vittoria is a mixture of Fock and Becke exchange with variable weight w, it is possible to study the dependence of E_G and U on w, which reveals the opposite natures of HF and LSDA (or GGA) in approximating the electron-electron correlation. Table IV presents a summary of these findings together with calculations of the exchange integral by Zuo and Vittoria [58].

This approach to calculating intrinsic ferrite properties provides a significant advance in understanding ferrite systems from a first principles approach and in accurately predicting exchange integrals, electronic properties, magnetism and thermomagnetic order.

In the next sections, we discuss high frequency applications and the needs and challenges for next generation microwave materials (Section IV), recent trends in processing of ferrite materials (Section V), and finally, as summary (Section VI) we will provide a perspective of ferrite materials and technologies as we face a new age of high frequency materials and technologies.

IV. FERRITE APPLICATIONS

As we have alluded to, it is because ferrite materials possess moderate to high magnetization, high permeability, moderate to high permittivity, and high electrical resistivity, that they are uniquely suited for high frequency applications over many decades of frequency. At lower frequencies, e.g., $\mathrm{dc} < f < 1\ \mathrm{GHz}$, ferrites commonly function as inductor cores in power generation, conditioning, and conversion, while at higher frequencies, e.g., $1\ \mathrm{GHz} < f < 100\ \mathrm{GHz}$, they function as passive and active devices that send, receive and manipulate electromagnetic signals. Other applications not falling into these categories include EMI shielding and absorbers, among others. Here, we largely limit our scope to off-resonance ferrite devices operating from $\sim 0.01 < f < 100\ \mathrm{GHz}$.

Ferrites find a wide variety of uses in military and commercial radar and communication electronics as integral materials

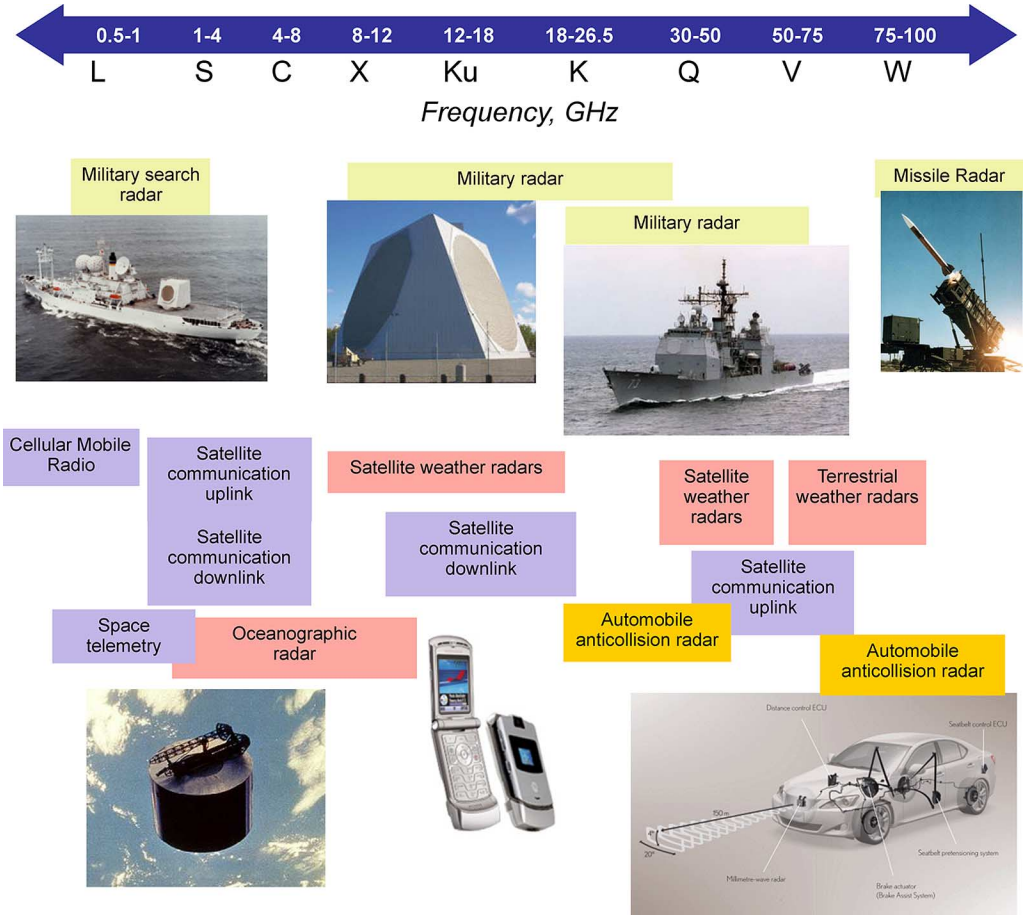

Fig. 5. Varied rf, microwave, and millimeter wave applications as they appear across the frequency spectrum from L to W bands.

in traveling wave tubes, switch mode power supplies, transformers, power converters, inductor cores, filters, etc. as well as passive electronics used in transmit and receive modules in isolators, circulators, phase shifters, filters, directional couplers, power limiters, etc.

Radar applications have obvious military applications but may also be used in commercial systems for applications in commercial aviation, severe weather warning radar, oceanographic satellite radar, and automobile anti-collision radar. Other applications include satellite communication uplinks and downlinks over a broad range of frequencies (see Fig. 5).

In the quest to take advantage of ferrite dielectric properties, as early as mid-1950s a wide variety of microwave ferrite devices, including circulators, isolators, phase shifters, directional couplers, power limiters, etc. based on polycrystalline spinel ferrites, were reported [62]. Early on it was understood that the FMR linewidth played a large role in determining magnetic loss and performance of rf and microwave devices [63]. The introduction of a new family of rare earth ferrites of the garnet structure possessing very low FMR linewidths was very significant [24], [64].

Ferrites of hexagonal crystal structure were identified as candidates for application at higher frequencies due to the high magnetic anisotropy fields that serve to shift the FMR frequency of these materials to the microwave and millimeter-wave bands [65].

Fig. 5 presents a frequency scale from ∼0.5 to ∼110 GHz in which different applications are presented, circa 2000. The applications include a broadband assortment of military and commercial systems and technologies including military radar, commercial radar, military and commercial communication, and automotive anti-collision radar, to name a few. This figure naturally omits the many classified military applications that span these frequency bands.

We next examine the materials needs of microwave devices. We limit ourselves here to those devices that are based on magnetic materials to provide necessary permeability, non-reciprocal behavior and self bias, among other properties.

A. *Microwave Materials Property Needs*

The specific needs of ferrite materials for microwave devices naturally vary depending upon the intended use of the materials. One challenge to scientists and engineers is the chasm that exists between the vernacular employed by engineer and physicist (or chemist, materials scientist, etc.). Often the functional needs of the microwave engineer are not easily communicated to the solid state physicist whom design ferrite materials, and visa versa. For example, the microwave engineer may require an insertion loss of less than 1 dB for a Y-junction circulator at X-band frequencies. To the physicist/materials scientist this constraint is difficult to translate to properties that they have control over in the design and processing of ferrite

materials such as anisotropy fields, coercivity, magnetization, etc. However, we have shown by iterative finite element method (FEM) designs, in which the FMR loss of the material (as FMR linewidth) is adjusted, that a 1 dB insertion loss roughly correlates to an FMR linewidth of nearly 700 Oe (at X-band). This rather crude demonstration depends upon other critical factors such as the operational frequency band relative to FMR, impedance matching, and conductive losses (among others) that may not be included in the linewidth calculation. The FMR linewidth in turn depends upon the intrinsic magnetic anisotropy and extrinsic parameters such as crystal quality, grain orientation, porosity, etc. [66] The later properties are often reflected in the coercivity of the ferrite that in turn has been shown to determine in part the remanent magnetization leading to self-biased properties. The operating frequency is often determined by the FMR frequency that is dependent upon the magnetization, anisotropy field, and applied magnetic fields. Both magnetization and anisotropy field are determined in part from atomic and electronic parameters and interactions. For example, fundamental sources of anisotropy include: magnetocrystalline, dipolar, spin-orbit coupling, single ion, pair-order, etc. These in turn are affected by the proportion, type and valence of cations, as well as the bond angle and distance between cations and anions. Point, line, and volume defects also contribute to changes in exchange which in turn affect magnetic anisotropy, magnetization, thermomagnetic behavior and FMR linewidth. In this way, one can appreciate the care in preparation that must be afforded magnetic materials for use at ultrahigh frequencies.

This correlation between engineering, or functional performance, and underlying physical properties is essential to the development of advanced materials that will address next generation microwave engineering needs.

Prior to the 1980s, ferrite materials were prepared predominantly in bulk form and often as powders and used principally as compacts and cores. During the late 1980s to early 1990s, ferrite materials were developed for the first time as thin films using such techniques as magnetron sputtering, pulsed laser deposition, and liquid phase epitaxy. Sputtered ferrites, having polycrystalline microstructures, found utility in early generations of magnetic recording media [67]. Typically films deposited by this technique possess copious grain boundaries (valued for recording media) leading to excessive dc and rf losses and little application value at microwave frequencies. However, recently, hexagonal barium ferrite films were deposited on Si (111) substrates by radio-frequency magnetron sputter deposition for possible microwave frequency applications. The films exhibited strong c-axis perpendicular orientation benefiting from a Pt buffer layer revealing ferromagnetic resonance linewidths, ΔH, 400–600 Oe at 40–60 GHz [68]. Although these properties hold promise for microwave applications, this technique tends to produce films of limited thickness, 200–500 nm, which make it ill-suited for many microwave applications.

Pulsed laser deposition, a technique that was developed and applied largely to oxide-based superconductors, has been applied to ferrite systems with great success [69], [70]. As will be discussed in the next section, PLD is effective at producing near single crystal quality thin films but is largely relegated to research studies since the films, like in sputter deposition, are limited in thickness. PLD also suffers from limited substrate surface area. Processing techniques leading to thick films, coatings, and layers, such as liquid phase epitaxy (LPE), screen printing, tape casting, and ceramic compaction, remain the dominant means of industrial scale processing of ferrite materials for high frequency commercial and military applications. For microwave passive device deposition tools must provide control of the direction and amplitude of the magnetic anisotropy field, FMR linewidth, remanent magnetization, and importantly, the film/substrate thickness to greater than 10s of microns. A paradox is faced in the refinement of ferrite materials in that many of these properties are optimized by the growth of near single crystal structures (e.g., anisotropy fields and low FMR linewidths) whereas other properties (e.g., high remanent magnetization needed for self-bias operation) require high coercive fields that are often inherent in materials having copious grain boundaries and defects. This dichotomy requires compromise in the choice of materials processing methods and conditions. The fact that these materials must be 10s of microns in thickness provides additional challenges.

So far, we have been most concerned with devices operating off resonance in which high permeability, high magnetization, and low FMR linewidth are highly valued. In contrast, for the case of electromagnetic interference (EMI) suppression and absorbers, material properties require high permeability but also high losses that readily allow for broadband absorption of electromagnetic signals. It is also desirable to either deposit magnetic materials directly over circuit board elements or create flexible sheets that can be affixed over radiating elements. These processing methods have until recently proven elusive. Materials processing technologies are discussed in greater detail in Section V of this review.

Having discussed materials needs, we next turn to key elements of transmit and receive modules for applications in radar and communication systems including circulators, isolators, phase shifters, filters, etc. In these elements there has been a trend towards microstrip designs. In Sections IV-B, IV-C, and IV-D, we discuss the merits of ferrite-based microstrip device designs keeping in mind that there exists a plethora of devices and topologies that include prominantly waveguide, transmission line, and stripline.

B. Circulators and Isolators

Our discussion of devices begins with a brief description of the microwave isolator as a transmission line with nonreciprocal attentuation. In its most simplistic manisfestation, it consists of a conductor positioned over a magnetic material, typically a ferrite, biased by an external magnetic field aligned perpendicular to the plane of the device and conductor. Although ferrite isolators consist of these basic elements they can operate on differernt principles: Faraday rotation, field displacement, and resonance absorption [71]. Most isolators make use of resonant absorption (or FMR). In contrast, a circulator has three of more ports and the nonreciprocal properties of the ferrite lead to standing waves that shunt electromagnetic power from one port to another while isolating the third.

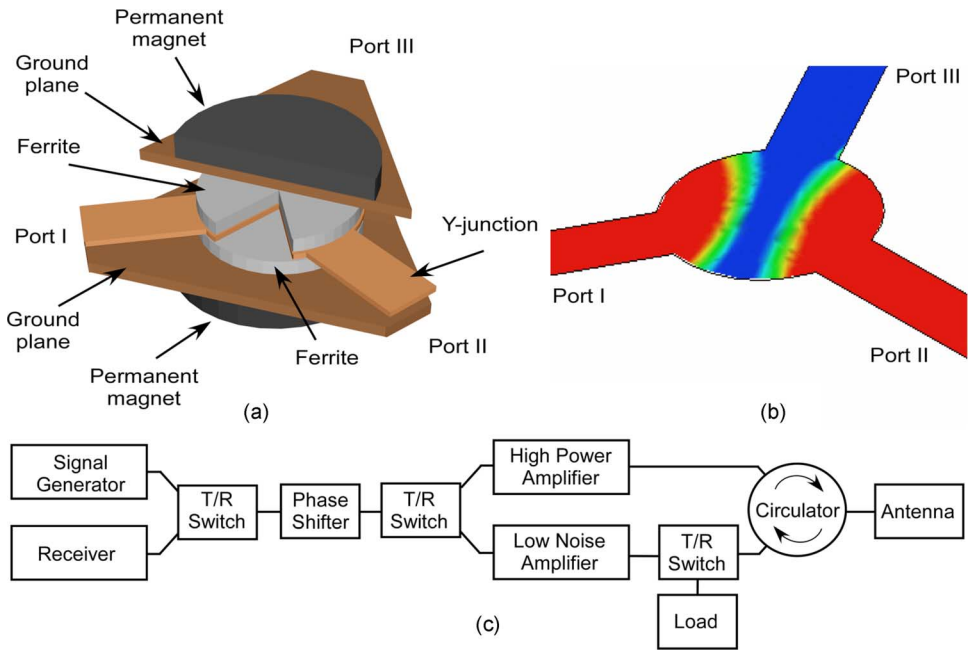

Fig. 6. (a) Components of a stripline Y-junction circulator. Permanent magnets provide the magnetic field necessary to bias the ferrite-loaded junction. (b) Magnitude of the electric field in the stripline Y-junction circulator calculated by finite element methods. Low insertion loss in the forward direction of propagation (port I–port II) and high isolation in the reverse direction (port I–port III) are observed. (c) Simplified block diagram of a T/R module. Switches and a circulator are utilized to guide the high power transmitted signal to the antenna in the transmit mode and to guide the low power signal from the antenna to the low noise amplifier and the receiver in the receive mode. The circulator also serves to protect the high power amplifier by dissipating the power reflected from the radiating antenna in the load. (Used with permission of the authors, [87]).

The frequency dependent permeability of ferrites, including spinels, garnets, and hexaferrites, assumes a tensor form due to the gyromagnetic nature of ferrites. Because the direction of precessional motion of magnetic dipole moments is dependent upon the sense of rotation for a given magnetic bias field direction, reversing the field direction reverses the sense of rotation. Hence, the rotational motion does not obey time reversal symmetry and results in non-reciprocal wave propagation properties. The frequency of the precessional motion, i.e., the ferromagnetic resonance (FMR) frequency, is proportional to the magnitude of the magnetic bias field, in addition to the externally applied magnetic field, the demagnetizing field and the magnetocrystalline anisotropy field. Since reversing the propagation direction is equivalent to reversing the sense of rotation in a circularly polarized wave, only one propagation direction will interact strongly with the ferrite. This direction-dependent nature of wave propagation in ferrite materials allows various non-reciprocal behavior such as that observed in isolators and circulators [85]. The strength of the interaction between the ferrite and the wave can be controlled by an external field, allowing various tunable devices, such as phase shifters and filters. The strongest interaction occurs at FMR, resulting in a strong attenuation of the wave. This property of ferrites is exploited in the design of various absorber devices.

We next examine the isolator/circulator as a key ferrite control element that finds a wide range of applications in the transmission, reception and manipulation of electromagnetic signals. The use of isolators play an important role in radar systems where they are used to control the voltage standing wave ratio (VSWR) seen by amplifiers and to mitigate reflected power from the antenna. In this case, dedicated isolators (2 port nonreciprocal devices) or circulators (3, or more, port nonreciprocal devices) can be used. In the case of a circulator, the third port is terminated by a matched load thereby allowing operation as an isolator. Depending upon system needs, space, and volume, dedicated isolators may be more desirable.

The circulator, one of the most frequently utilized ferrite devices in modern microwave systems, is a passive non-reciprocal multi-port device used to control the power flow and to isolate various components in high frequency systems. For example, the Y-junction circulator, depicted schematically in stripline configuration in Fig. 6(a), is often utilized in transmit-receive (T/R) modules that shape and steer the beam of phased array radar systems [72]. T/R modules, a simplified block diagram of which is shown in Fig. 6(c), combine monolithic microwave integrated circuits (MMIC) and digital circuitry fabricated on high frequency semiconductor substrates, such as gallium-arsenide and gallium nitride, to produce high performance, high efficiency, low weight, low cost, and small size modules [73]. In many modern T/R modules the one arm of the circulator has a matched load and the circulator acts as an isolator. In this case the send and receive functions are switched as opposed to being operated in a STAR mode (simulatneous transmit and receive).

The ferrite is the material that interacts strongly with the EM signal and provides non-reciprocal behavior. Nonreciprocal microstrip devices such as isolators and circulators require the ferrite to have a magnetization vector aligned perpendicular to the device/film plane. A relatively new circulator design, the ferrite coupled line circulator, allows for in-plane alignment of the magnetization but suffers from higher insertion loss and therefore has yet to become a viable option to the Y-junction circulator.

The first waveguide Y-junction circulators were reported in the late 1950s [74] with stripline designs following soon thereafter [75]. The first monolithic microstrip circulator on a garnet substrate was introduced in 1967 [76]. The theory of stripline Y-junction circulators was developed by Bosma [77], [78], and Fay and Comstock [79]. These theories explain the non-reciprocal behavior of the ferrite loaded stripline Y-junction in terms of the splitting of counter-rotating dielectric resonance modes in the ferrite material due to the off-diagonal elements of the permeability tensor proposed by Polder [80], [81].

Typical electric field configuration in the ferrite-loaded stripline Y-junction computed by finite element methods is shown in Fig. 6(b). Here one sees the stabilization of a standing wave that acts to shunt the flow of power from one port to another while concomitantly isolating the third. The conditions necessary for circulation over a full octave bandwidth in microstrip devices were demonstrated by Wu and Rosenbaum [82]. The extensive literature on circulator theory and design is reviewed in the annotated bibliography by Knerr [83] and in books by von Aulock and Fay [84] and Helszajn [85].

The need to miniaturize circulator devices, to facilitate broader integration with monolithic microwave circuits and to extend the applicable frequency range into the millimeter-wave regime, has motivated studies in utilizing the unique properties of hexagonal ferrites. Textured polycrystalline hexagonal ferrites, such as barium and strontium hexaferrite, can be produced with permanent magnet properties such that they will remain in a stable magnetized state in the absence of an external bias field (i.e., self-biased). High uniaxial magnetic anisotropy fields in these materials, which can exceed 40 kOe, are utilized to decrease or eliminate the external biasing field requirement according to Kittel's [86] resonance equation that incorporates both dipolar and magnetocrystalline anisotropy interactions [87].

Polycrystalline textured strontium hexaferrite $(\mathrm{Sr}M)$, having a remnant magnetization of approximately 3.5 kG, uniaxial anisotropy field of 18.4 kOe, and FMR linewidth of approximately 2 kOe, was utilized to develop a self-biased waveguide junction circulator operating at 73.5 GHz by Akaiwa and Okazaki [88]. The reported insertion loss was 1.1 dB with isolation exceeding 20 dB over a 2.4 GHz bandwidth. In 1989, polycrystalline $\mathrm{Sr}M$ was utilized to develop a self-biased waveguide circulator operating at 30.7 GHz with an insertion loss of less than 1 dB and isolation of more than 20 dB over a 1% bandwidth [89]. In 1992, a textured barium/strontium ferrite with remanent magnetization of 3.5 kG and uniaxial anisotropy field of 21 kOe was utilized to design microstrip and stripline circulators operating at 37 and 32 GHz, respectively [90]. In 2001, an integrated self-biased microstrip circulator was fabricated through bonding of textured $\mathrm{Sr}M$ platelets to silicon substrates in a low temperature process compatible with semiconductor fabrication protocols [91]. Insertion loss of 2.8 dB and isolation of 33 dB were measured at 28.9 GHz with a 20 dB bandwidth of 1%. Circulator designs utilizing single crystal platelets of $\mathrm{Sc}M$ with saturation magnetization of 3.9 kG, uniaxial anisotropy field of 8.7 kOe and linewidth of 100 Oe embedded into glass-microwave integrated circuit wafers resulted in operation at 22.2 GHz with a minimum insertion loss of 2 dB and isolation of 21 dB. This performance was obtained with ferrite platelets partially saturated by an externally applied magnetic field of 2 kOe (55% saturation) [92], [93]. Recently, Wang *et al.* [94] developed a self-biased Ku-band circulator. This two dimensional construct employed a self-biased $\mathrm{Sr}M$-type hexaferrite and demonstrated an insertion loss of less than 2 dB with a corresponding isolation of 20 dB over a bandwidth of 500 MHz with a center frequency of 13.5 GHz. This was the first such demonstration of a self-biased circulator operating at a frequency less than 20 GHz.

As mentioned previously, the circulator design that has the most potential for monolithic microwave circuit integration and self-bias operation is the ferrite-coupled-line (FCL) circulator. First developed in the 1980s, in contrast to Y-junction circulators, FCL circulators utilize longitudinally magnetized ferrite to couple modes between closely spaced wave guiding lines [95]. The non-reciprocity of ferrite coupled waveguides was first explained in terms of coupled mode theory by Marcuse [96].

FCL circulators have the additional advantages of broad bandwidths, planar form factors, and smaller biasing field [97]. Self-bias designs utilizing hexagonal ferrites have also been reported [98]. Due in part to a lower demagnetizing factor associated with a longitudinally magnetized film, self-biased hexaferrite films are easier to produce to thicknesses necessary for FCL device fabrication. Therefore, self-biased FCL circulators have the potential for true monolithic integration where the ferrite film is deposited and metalized with proper circuitry during device fabrication. There is no doubt that circulator designs described here, as well as other high frequency ferrite devices, will continue to benefit from further advances in ferrite materials to result in true microwave monolithic integrated circuits.

C. Phase Shifters

Phase shifters are critical elements for electronically scanned phased array (ESPA) antennae and are devices that allow the antennae beam to be steered without physically re-positioning the antennae. Existing phase shifter technologies, for example, ferroelectric, semiconductor-MMIC, and MEMS each suffer shortcomings or operational constraints that limit their wide scale deployment across varied military and commercial platforms (see Table V for comparison of existing phase shifter technologies [99]). The key figures of merit include: phase shift per dB of insertion loss, power budget, power handling, and size, weight, and cost. Here, we target phase shifter applications in which high performance is demanded in low profile—lightweight devices that handle high power loads (10s Watts average power). Such applications include radar and communication phased array systems on aircraft, satellite, ships, and importantly, next generation unmanned systems. Fig. 7 illustrates, for example, the power budget of a transmit chain for an L-band T/R module for a satellite communication active phased array system. Of the key elements, the semiconductor-based phase shifter introduces a disproportionate loss. Clearly, enhanced T/R module performance would be realized by the reduction in insertion loss of phase shifters. This is one driving force in the development of next generation phase shift device technology. Semiconductor phase shifter technologies

TABLE V
COMPARISON OF PHASE SHIFTER TECHNOLOGIES

	Ferroelectric	MEMS	Semiconductor	Ferrite (waveguide)	Ferrite (microstrip)
Cost	Low	Low	High	Very high	Low
Reliability	Good	Good	Very good	Excellent	Excellent
Power handling	>1 W	<50 mW	>1 W	~1 kW	>10 W
Switching speed	~ ns (limited if high voltage)	10 - 100 μs	< ns (low power)	10 - 100 μs	<10 μs
Radiation tolerance	Excellent	Excellent	Poor (good if hardened)	Excellent	Excellent
DC power consumption	~ 1 μW	Negligible	<10 mW	~10 W (~1 W latching)	<10 μW
Microwave loss	~ 5 dB/360° K band	~2.3 dB/337.5° Ka band	~ 2 dB/bit Ka band = 8 dB	<1 dB/360° X band	<2 dB/360° C - Ku bands
Size	Very small	Small	Small	Large	Small

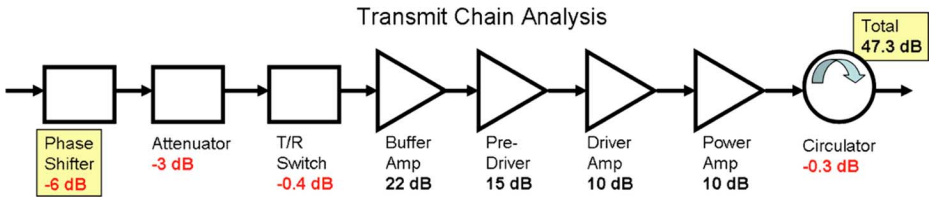

Fig. 7. The power budget of a transmit chain for an L-band T/R module for a satellite communication active phased array system. Of the key elements the semiconductor-based phase shifter introduces a disproportionate loss.

(i.e., diode and FET-based) suffer from low power handling (<1 W), high power dissipation (1–2 W), high insertion loss (6–8 dB at X-band), poor phase resolution (~4 bits), and often-costly hermetic packaging. As target frequencies approach and surpass Ku band, increases in IL due to conduction losses in the semiconductor become prohibitive. Benefits of semiconductor phase shifters include broadband operation and low cost. In comparison, advantages of existing ferrite phase shifter technology include very low-loss operation, <1 dB, high power handling capabilities (100s W_{ave}, 1000s W_{pk-pk} for waveguide technology), reliability and radiation hardness. However, these devices are large/heavy, require large power budgets (up to 10 W), and are costly to fabricate. As a result they are used principally in specialized applications such as high power passive phased arrays.

Recent breakthroughs in microwave materials and device technologies include:

(i) the ability to process near single crystal quality ferrite thick films and ceramic compacts suitable for application in ultra-low loss microwave passive device applications;
(ii) the ability to process high quality ferrites having self-biased properties while maintaining low microwave losses;
(iii) microstrip passive phase shifter designs that require significantly smaller bias fields;
(iv) computational advances that have set the groundwork to successfully and accurately describe EM wave propagation in highly anisotropic magnetic materials; and
(v) novel voltage and current driven transducer technologies that produce magnetic bias fields that enable active tuning of devices with minimal power loads.

The phase shifter technology described herein combines the low-loss, high power handling, reliability, and radiation hardness of today's ferrite waveguide phase shifters in a planar, cost-effective, high power handling—low power consumption microstripline topology. In contrast to other phase shifter technologies, ferrite phase shifters are characterized as having superior insertion loss performance and microwave power handling capabilities. These devices are also highly reliable and radiation tolerant—properties valued for space related applications. Ferrite phase shifters rely on electromagnetic wave propagation in low-loss magnetic materials, such as yttrium iron garnet (YIG) and spinel ferrites, typically substituted with nonmagnetic cations of lithium, magnesium, nickel, and zinc. Such devices require magnetic fields to bias and actively tune phase angle. These fields may be generated by permanent magnets for static bias fields or current-driven coils for dynamic tuning. For operation at high frequencies (at or above X-band), permanent magnets are large, heavy and costly. Tunable ferrite components, in addition to being comparatively large, experience high DC power consumption and slow response times due to the large inductance of current-driven coils. Improved response time and reduced DC power consumption are achieved in latching-type ferrite phase shifters where short current pulses are used to set the phase [87].

A recent development that may significantly impact the tuning of microwave magnetic devices is multiferroic (MF) materials exhibiting the magnetoelectric (ME) effect [100]. Among the numerous investigations appearing in the literature, multiferroic (MF) metamaterials, constructed as multilayered or granular heterostructures, have drawn the

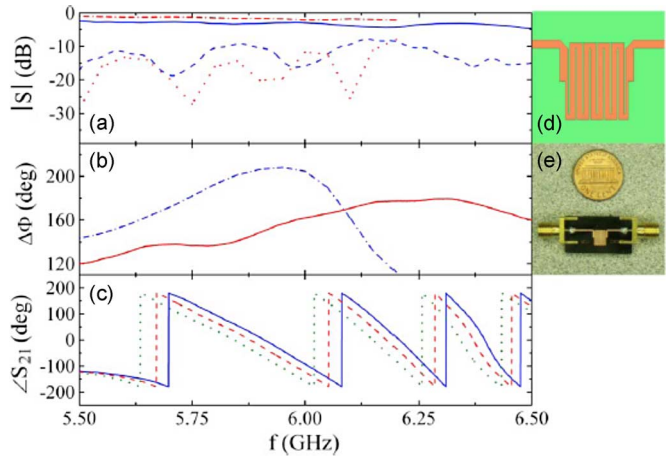

Fig. 8. a) Calculated dotted dashed and measured solid insertion loss. Calculated (dotted) and measured (dashed) return loss. b) Calculated (dotted dashed) and measured (solid) differential phase shift. c) Measured insertion phase at an applied electric field of 0 (solid), 3 (dashed), and 6 (dotted) kV/cm. d) Finite element model of the microstrip circuit. e) Fabricated device with coaxial edge mount SMA connectors. (Used with permission of the authors, [106]).

most attention [101]. Multiferroic heterostructures have indeed been shown to offer unique opportunities in the development of many new multifunctional devices, including electric-field-controlled (EFC) magnetic memory elements [102]. EFC microwave devices [103] and E- and H-field transducers having magnetically modulated piezoelectricity or electrically modulated magnetoelectricity [104], [105]. In many of these examples, mechanical coupling between piezoelectric (e.g., PZT, PMN-PT, etc.) and magnetostrictive (e.g., Terfenol-D, Galfenol, Metglas, etc.) layers provides electric field induced magnetic polarization of the magnetostrictive layer(s) and magnetic field induced electric polarization of the piezoelectric layer. Alternatively, Geiler *et al.* [106] have demonstrated the generation of magnetic fringe fields by MF heterostructures that act on nearby microwave devices that are decoupled from the transducer. In both instances the MF heterostructures may eliminate the need for voluminous and costly magnetic field coils to actively tune magnetic components. These developments represent a disruptive advance in the field of multifunctional electronics.

Geiler's voltage tuning of a meander line ferrite phase shifter (see Fig. 8(d) and (e)) was realized by affixing a YIG substrate to a MF heterostructure consisting of PMN-PT/Terfenol-D/PMN-PT. This geometry allowed the YIG substrate to see the voltage induced magnetic fields emanating from the MF heterostructure without experiencing any strain or microwave electromagnetic coupling. A magnetic bias field of 200 Oe was applied along the length of the MF heterostructure, and along the meander line elements, by an electromagnet. Measured insertion and return loss are superimposed with calculated spectra in Fig. 8(a). At a frequency of 6.3 GHz, the insertion loss and the return loss were measured to be 3.2 and 13 dB, respectively, while a differential phase shift of 180° was measured at 6.3 GHz. Out of the 3.2 dB of insertion loss, 0.5 dB is attributed to impedance mismatch loss. The remaining 1 dB between calculated and measured insertion loss is attributed to connector effects, imperfections associated with the device fabrication process, and variations in the material properties from those assumed in the finite element model. The contribution of the MF heterostructure to the insertion loss was less than 0.2 dB. The magnetic fringe field was nonuniform and varied from 330 Oe near the edge of the 1.3 cm YIG substrate to 210 Oe near the center. Differential phase shift was calculated by subtracting the insertion phase at zero internal field from the insertion phase at 100 Oe internal field. A differential phase shift of 210° was calculated at the design frequency (Fig. 8(b)). As the electric field increased from 0 to 6 kV/cm, a linear tunable phase shift of more than 65 degrees was observed (Fig. 8(c)). This phase change was due to the fact that the magnetic fringe fields from MF heterostructure varied by approximately 20% with applied electric field. These results demonstrate the potential of MF heterostructures as external tuning elements for microwave magnetic devices.

A different path was taken by Tatarenko, *et al.* [107] who demonstrated an electric field tunable yttrium iron garnet YIG-lead zirconate titanate PZT phase shifter based on the tuning of ferromagnetic resonance at X-band. The electric field control of the phase shift arose through a magnetoelectric interaction in which a piezoelectric deformation in PZT occurred under the application of an electric field E leading to a shift in the FMR frequency in YIG. A phase shift of 90 to 180° and an insertion loss of 1.5–4 dB was measured corresponding to an $E = 5$–8 kV/cm applied across PZT. This approach represents a new path towards realizing high performance EFC phase shifter devices.

The discovery of metamaterials possessing negative index of refraction (NIM) has allowed for the development of novel microwave technologies [108]. A significant recent development is the fabrication of tunable negative index metamaterials (TNIM) utilizing high quality ferrite materials [109]–[113]. One such example of a microwave device making use of a ferrite-based TNIM is the He *et al.*, phase shifter [111], [112]. As discussed previously, there is significant demand in the microwave industry for affordable, light weight, high power phase shifters. In ferrite phase shifters a change in permeability by the application of magnetic field causes a change in the phase velocity of the microwave signal traveling through the phase shifter. Traditional ferrite phase shifters operate at frequencies far from the FMR in order to avoid absorption losses. As a result, the real part of the complex permeability, μ', is necessarily small. Experimental and theoretical investigations of field tunable negative refractive index metamaterial (NIM) using a yttrium iron garnet (YIG) films and an array of copper wires in waveguides were carried out by both P. He *et al.* and Y. He *et al.*: A key feature of magnetic field tunability of the NIM in the microwave frequency region was demonstrated [109], [110]. Transmission passbands were realized in the negative refractive index region that could be tuned by an external magnetic field. The permeability of the NIM was simultaneously tuned along with the refractive index. The change in permeability leads to a change in the phase velocity of the signal and, therefore, the phase of the transmission coefficient.

The advantage of using a ferrite NIM for phase shifter applications is that it allows for low-loss operation over frequencies near FMR where μ' is negative and relatively high. In the field

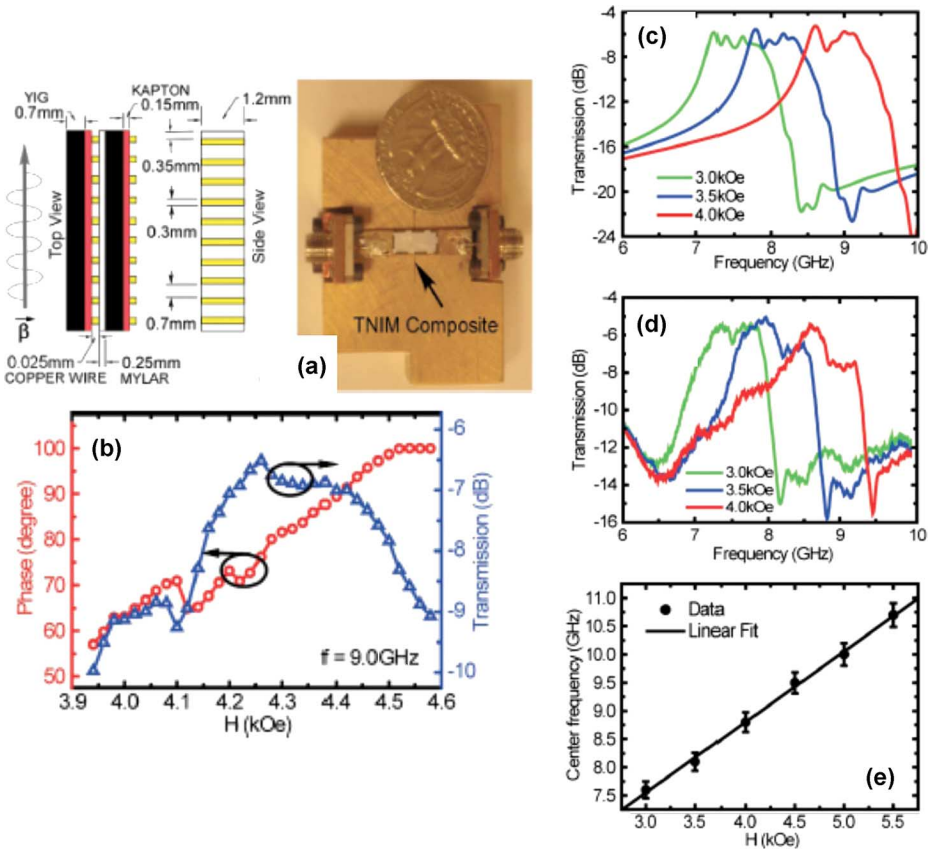

Fig. 9. a) Schematic top and side views of the $10.0 \times 2.0 \times 1.2\ \mathrm{mm}^3$ TNIM composite. Photograph of the microstrip test fixture, a $5 \times 25\ \mathrm{mm}^2$ upper strip on the brass ground base relative to a U.S. quarter provided for a visual size comparison. The TNIM composite is mounted under the center of the upper strip. b) Measured phase shift and corresponding transmission vs. the magnetic bias field of the TNIM composite at 9.0 GHz. The insertion phase shifts 45° while the transmission varies from −6 to −10 dB. c) Simulated and d) measured 1.0 GHz wide TNIM passbands of over −8 dB transmission centered at 7.5, 8.0, and 8.8 GHz at magnetic bias fields of 3.0, 3.5, and 4.0 kOe, respectively. e) Center frequency of the TNIM passband increases linearly from 7.6 to 10.7 GHz with the bias field changing from 3.0 to 5.5 kOe. (Adapted from [112].)

tunable NIM, the effect of the ferrite is to provide a tunable negative permeability over a continuous range of frequencies on the high frequency side of FMR. Complementary negative permittivity, ε', was achieved using a single periodic array of copper thin film wires deposited on Kapton. A negative refractive index region of 0.5 GHz in width at K band was demonstrated. Increasing the volume of the YIG increased the absorption and therefore a tradeoff between bandwidth for the negative index region and low-loss was realized. Additionally, the dielectric permittivity of the YIG slabs reduced the effective negative permittivity obtained from the plasmonic copper wires. For a 1 cm long NIM, when the applied magnetic field was varied from 6.0 to 7.0 kOe, the phase varied 160° with the insertion loss varying from 4.3 dB to 6.3 dB at 24 GHz.

A tunable negative refractive index metamaterial and miniature phase shifter were also designed and fabricated in a microstripline configuration for applications in rf, microwave and millimeter wave integrated circuits [111]–[113]. The metamaterial consisted similarly of plasmonic copper wires and YIG slabs having an insertion loss of 5 dB at the center of the transmission band. The YIG enabled magnetic field tuning of the negative refractive index from 7.0 to 11.0 GHz. The insertion phase was tuned by 45° continuously by varying the bias field from 3.8 to 4.6 kOe at 9.0 GHz. Fig. 9(a)–(e) illustrate a schematic of the device with photograph (see Fig. 9(a)) and the devices phase shift and transmitted signal (i.e., passband) (see Fig. 9(b)). In Fig. 9(c)–(e) one sees the simulated and experimental passbands signaling the occurrence of negative index. This passband was shown to shift under the application of a magnetic field demonstrating broadband tunability of the NIM. H-field tuning was shown to be broadband and linear, see Fig. 9(e).

Finally, a similarly structured tunable negative index metamaterial was designed, fabricated, and tested in a Q-band rectangular waveguide [113]. The structure consisted of a single crystalline scandium-doped barium hexaferrite $(\mathrm{Sc}-\mathrm{Ba}M)$, aligned parallel to two rows of periodic copper wires (see Fig. 10(a) and (b)). The magnetic field tunable passband was measured indicating the occurrence of the negative index. The center frequency of the 5 GHz wide passband, having a transmission peak of −13 dB, was shifted linearly from 40.9 to 43.9 GHz by varying the bias field from 4.0 to 7.0 kOe (see Fig. 10(c) and (d)). These examples of TNIM-based electronic components represent a new approach in the design and fabrication of miniature microwave passive devices that rely upon tuning the permeability spectrum in frequency space near FMR.

D. Filters

Microwave filter designs have been a topic of great interest for more than seven decades [114] and continue to grow as high

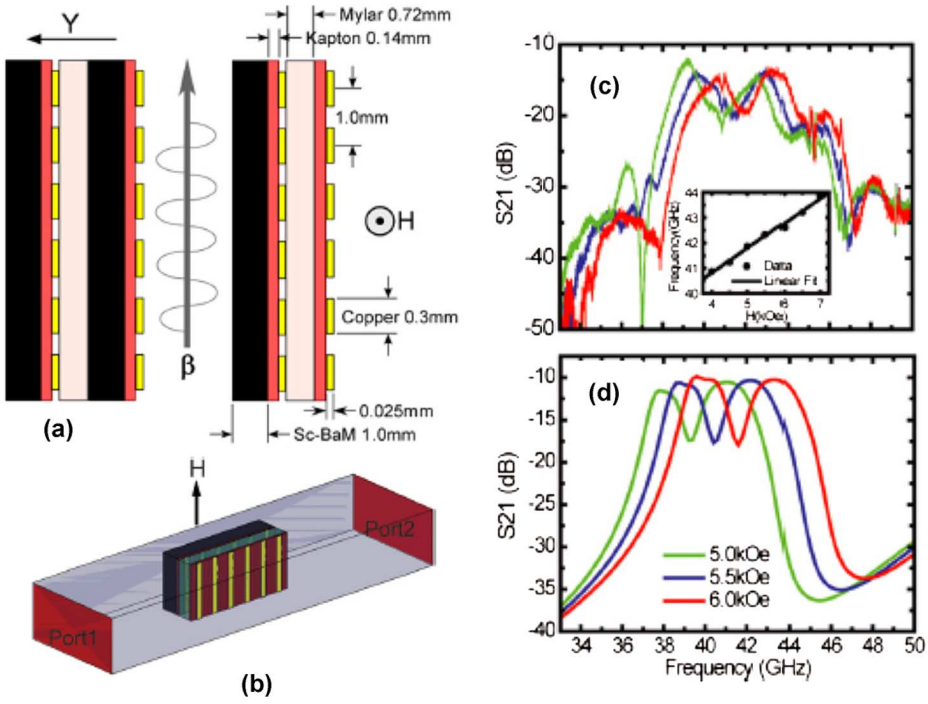

Fig. 10. a) Top views of the TNIM design consisting of two Sc-BaM slabs, two rows of copper wires on Kapton substrate, and a Mylar spacer and the simplified TNIM consisting of only one Sc-BaM slab. The magnetic bias field H, the propagation constant β and the directional vector from copper wires to their vicinal ferrite slab Y form a right-handed triplet. (b) The schematic drawing of the TNIM composite mounted in a Q-band rectangular waveguide. c) Measured and (d) simulated S21s of the TNIM composite containing a 1.0 mm thick Sc-BaM slab under bias fields of 5.0, 5.5 and 6.0 kOe, respectively. Inset: measured centre frequency of the TNIM passband versus the magnetic bias field. (Adapted from [113].)

performing materials and increasingly complex designs are investigated to meet stringent modern-day requirements. A major development to the field of microwave filters was the advent of tunable bandwidth parameters allowing for a single device to operate at user-defined frequencies [115]. The tuning mechanisms in these filters vary from static mechanical methods such as plungers, screw-tuned cavities, and conductor-conductor positioning, to active methods such as applied E-field and H-field tuning, with each method offering distinct benefits [114], [115]. Active methods, such as E-field and H-field tuning, allow for remote device performance tuning as well as the ability to automate band tuning for frequency-modulated applications. Active tuning also enables high-speed precision band pass adjustments and better repeatability than mechanical tuning methods. The advantages of H-field tunable filters over E-field tunable varactor or MEMS devices include low insertion loss and high power handling. YIG filters, based on single crystal resonators, are among the most widely utilized H-field tuned devices offering multi-octave band tunability and high Q-factors.

Next, we examine a highly versatile, planar, low-loss, and low cost alternative to YIG single crystal resonator filters with a low externally applied H-field requirement. The proposed design consists of a 5-pole Chebyshev bandpass filter implemented in microstrip hairpin-line coupled resonator geometry on a polycrystalline YIG substrate biased and tuned with an externally applied H-field above the FMR frequency (see Fig. 11(a)–(c)) [116].

The hairpin-line bandpass filters are essentially parallel-coupled half-wavelength resonators folded into a "U" shape and follow the same set of design equations that govern parallel-coupled half-wavelength resonator filters [115]. A 5-pole Chebyshev equiripple response is considered, however, Butterworth, elliptical, and other filter response types are equally applicable.

The dynamic tuning of the proposed device is realized by varying the magnetic permeability of the substrate by applying an external magnetic field. The variation in permeability with applied field is strongest below the FMR frequency and above the ferromagnetic anti-resonance (FMAR) frequency. Operation sufficiently far from both resonance conditions is necessary to achieve low-loss performance.

The measured insertion loss of a ferrite microstrip hairpin-line bandpass filter is compared with the predictions of the numerical model in Fig. 11(d). Good agreement in the frequency range of interest is observed. Under an externally applied field of 100 Oe, an insertion loss of 1.3 dB was measured at 8.8 GHz compared to 0.9 dB predicted by the numerical model.

H-field tuning of the ferrite microstrip hairpin-line bandpass filter is demonstrated (Fig. 11(e)). The device exhibits passband tunability with center frequency varying from 8.3 GHz to 9 GHz under applied H-fields of 50 to 200 Oe. The insertion loss at the passband center frequency varies between 1 and 1.4 dB as a function of applied H-field. While a bandpass filter design with a fractional bandwidth $(\Delta f / f_{\text{center}})$ of approximately 10% at X-band was demonstrated, the proposed approach lends itself to the realization of a broad range of filter responses, including lowpass, highpass, bandpass, and bandstop, as well as passband characteristics, including center frequency, fractional bandwidth, passband ripple, out-of-band rejection, etc. Furthermore, due to the low H-field requirement, the proposed filter design has the potential for high-speed and low-power operations,

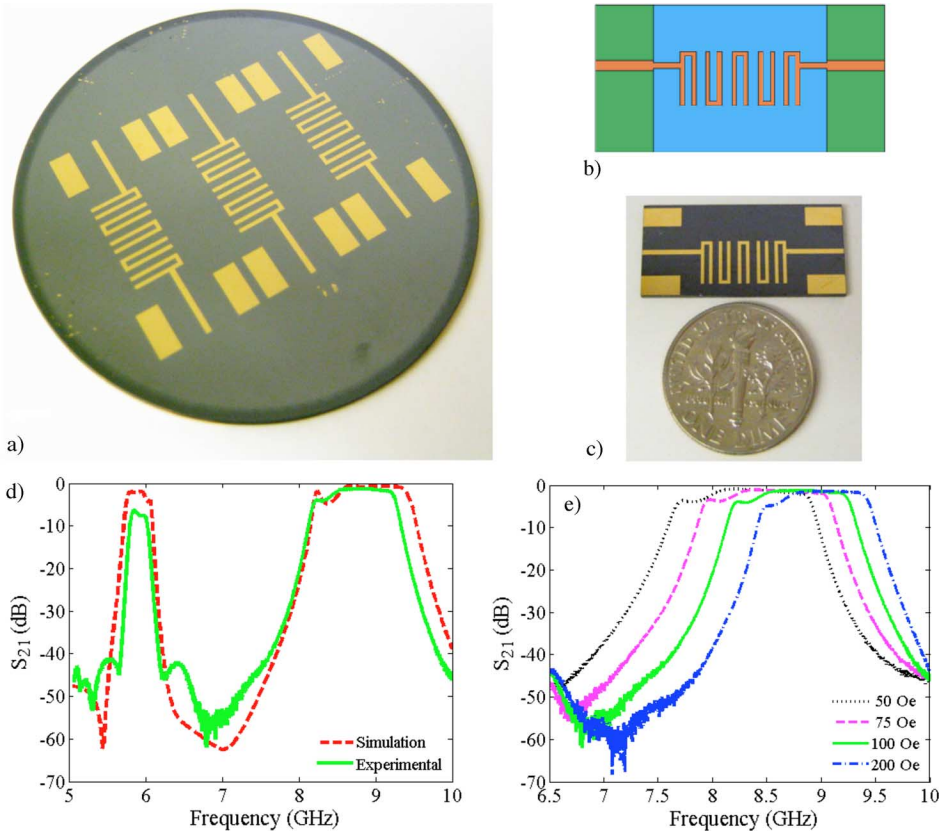

Fig. 11. (a) Photograph of patterned 50 mm diameter YIG wafer. (b) Outline of the hairpin-line resonator bandpass filter design used in numerical modeling. (c) Photograph of fabricated bandpass filter device. (d) Simulated and measured passband characteristics of the ferrite microstrip hairpin line coupled resonator bandpass filter. Measured spectrum is collected under applied magnetic field of 100 Oe. (e) Passband characteristics of the ferrite microstrip hairpin line coupled resonator bandpass filter under applied magnetic field from 50 to 200 Oe. (Adapted from [116].)

in addition to possessing radiation tolerant properties making them well-suited for space related applications [99].

Multiferroic (MF) heterostructures that demonstrate the magnetoelectric effect (ME) can also be adapted as tunable microwave filters [117]. ME resonators, consisting of 110 μm thick (111) yttrium iron garnet (YIG) on a GGG substrate bonded to PZT, have been demonstrated. In that example, YIG, having a saturation induction $4\pi\mathrm{M}$ of 1750 G and a FMR linewidth of $\sim$1 Oe, was bonded to a PZT plate poled in an electric field of 10 kV/cm perpendicular to the sample plane. The heterostructure consisted of a YIG film bonded to a PZT crystal with ethyl cyanoacrylate. The heterostructure was placed between transducers, and was subjected to a field H parallel to the sample plane and perpendicular to the microstrips. The frequency dependence on the insertion loss was measured from 4–10 GHz as a function of H and E fields applied across the PZT. The maximum ME coupling was observed at $f_\mathrm{r} = 6.77$ GHz corresponding to FMR in YIG. A frequency shift was observed and attributed to the strain at the YIG-PZT interface caused by the piezoelectric response of the PZT. A near-linear variation in δf with E was observed. A maximum shift of 120 MHz for $\mathrm{E} = 3\,\mathrm{kV/cm}$ corresponding to 2% of the center frequency of the filter was measured [117].

Next, we review popular and effective techniques of producing high quality ferrite materials as thin and thick films, powders, compacts, quasi-single crystals, and metamaterials.

V. Ferrite Materials Processing

Thin film ferrites are typically produced by physical vapor deposition (PVD) techniques that may include molecular beam epitaxy (MBE), chemical vapor deposition (CVD), sputtering deposition, and pulsed laser deposition (PLD). Alternatively, chemical hydrolysis using spin spray plating (SSP), or variants of the same, have also been explored and demonstrated as valuable techniques for producing thin and thick film ferrites under low temperature conditions.

Molecular beam epitaxial growth techniques result in very high quality single crystal, or quasi-single crystal ferrite films. MBE growth of ferrites has been driven by the pursuit to understand underlying physical phenomena of thin films of $\mathrm{Fe_3O_4}$ [118] and $\mathrm{CoFe_2O_4}$ [119] grown on MgO (001) and magnetoresistance in spin valve structures consisting in part of $\mathrm{Fe_3O_4}$ layers [120]. Recently, MBE has been applied to the $\mathrm{Ba}M$ hexaferrite system resulting in high crystal quality films grown on Mg(001)/SiC(0001) [121]. Although MBE finds great utility in the study of fundamental phenomena in ferrites, films suffer from very limited thicknesses of $\sim$10–200 nm that are impractical for most microwave and mm-wave applications.

A variety of chemical vapor deposition (CVD) techniques have been applied to the growth of ferrite film systems. CVD variants, including plasma assisted, metalo-organic, and injection-CVD (and combinations of these) were successfully applied in the growth of $\mathrm{Fe_3O_4}$ [122], [123] $\mathrm{Co_xFe_{3-x}O_4}$

films [124], NiZn-ferrites [125], and Ba-hexaferrites [126]. These techniques have been applied to realize films of several microns in thickness. Although thick in comparison to MBE, PLD, and magnetron sputtering, these thicknesses remain too thin for most high frequency applications. Further, these films tend to possess comparatively large FMR linewidths stemming from chemical impurity contamination. Because of these shortcomings, CVD has not yet become a mainstay technique for the growth of thick film ferrites for rf, microwave, and mm-wave applications.

Magnetron sputtering has been used principally for the deposition of granular ferrite films for applications in high density magnetic recording, etc. In the case of sputtering it is not uncommon to deposit ferrites as an amorphous phase that is then heat-treated beyond crystallization to obtain the desired morphology and structure for high-density data recording applications. Sui *et al.* [67] presents a review of these processes and resulting properties for Ba hexaferrite films. Spurred by the work of Sui *et al.*, Snyder *et al.* [127], [128] showed through the application of x-ray absorption fine structure that a local structural precursor within the amorphous film predetermines the crystalline texture of the hexaferrite films valued for memory storage.

For our discussion of thin film ferrites in Sections V-A and V-B, we limit our discussion to PLD and SSP since these techniques have been proven the most effective in processing a wide range of high crystal quality ferrite films attractive for high frequency applications.

A. Ferrite Films and Coatings Using Pulsed Laser Ablation Deposition

Pulsed laser deposition (PLD) is a well-established method for growing ferrite films. In conventional PLD, laser pulses from a high-energy laser, often an excimer laser, ablate a target material forming a molecular flux or plume. The substrate intercepts the plume allowing for the growth of films of similar composition as the target material on selected, often lattice matched, substrates. PLD has been used in the deposition of garnet, spinel, and hexaferrite ferrites among other oxides such as high temperature superconductors and magnetoresistive manganites. Growth of ferrite films using PLD was first proposed by Vittoria [70] in 1991. The PLD of yttrium iron garnet (YIG) films was first demonstrated by Dorsey *et al.* [129] Films with thicknesses of about 1 μm were deposited on (111) gadolinium gallium garnet (GGG) substrates. FMR linewidths of $<$1 Oe were observed in films deposited under oxygen pressures $<$250 mTorr and high substrate temperatures $> 800^{\circ}\mathrm{C}$. Films of $\mathrm{Bi_3Fe_5O_{12}}$ (BIG), $\mathrm{Eu_1Bi_2Fe_5O_{19}}$ (EBIG), as well as YIG/BIG and YIG/EBIG heterostructures, were investigated by Simion *et al.* [130]. Thick, $\sim$ 50 μm, epitaxial YIG films having linewidths of $\sim$5.7 Oe were deposited on (111) GGG substrates at a high rate by Buhay *et al.* [131] In the same paper 50–100 μm thick polycrystalline films where deposited on 3″ gold plated (100) Si wafers. The magneto-optical properties of Ce [132] and Bi [133], [134] substituted YIG films and YIG/GGG superlattices [135] grown by PLD on (111) GGG substrates have been investigated.

The first PLD-grown $\mathrm{Ba}M$ hexaferrite films were reported by Dorsey *et al.* in 1992 [129] In the years following many researchers applied PLD to ferrite film synthesis. Shi *et al.* [92] deposited Sc-doped BaM films on c-plane sapphire having the crystallographic c-axis aligned normal to the film plane. Among the highest quality $\mathrm{Ba}M$ films made were those by Song *et al.* [136] who achieved perpendicular magnetic anisotropy and an FMR linewidth of $\sim$16 Oe at 60.3 GHz.

Most research studies discussed thus far involving hexaferrites have strived to align the crystallographic c-axis perpendicular to the film plane. As was discussed previously, in-plane orientation can be achieved by using suitable substrates that are chosen for their close match to the film's lattice parameters and thermal expansion coefficients (e.g., a- or m-cut sapphire). Welch *et al.* [137] reported the growth of $\mathrm{Ba}M$ films having the crystallographic c-axis (i.e., magnetic easy axis) aligned randomly within the film plane, while Yoon, Vittoria and Oliver [138] subsequently reported the c-axis of the $\mathrm{Sc}M$ (scandium doped $\mathrm{Ba}M$) films aligned in the film plane parallel to the c-axis of the m-plane sapphire substrate.

PLD growth of spinel ferrites was first realized by Tanaka *et al.* in 1991 [69]. In that work, polycrystalline nickel zinc ferrite, $\mathrm{Ni}_x\mathrm{Zn}_{1-x}\mathrm{Fe_2O_4}$, films were deposited on glass substrates. Johnson *et al.* [139] reported the growth of nickel ferrite, $\mathrm{NiFe_2O_4}$, on c-cut sapphire substrates using both PLD and ATLAD (i.e., alternating target laser ablation deposition). Post-annealing was found to enhance the magnetic properties of these films including increasing the magnetization and reducing the FMR linewidthc [140].

Balestrino *et al.* [141] reported the PLD growth of lithium ferrite, $\mathrm{Li_{0.5}Fe_{2.5}O_4}$, and Mn and Zn-doped lithium ferrite films. Cillessens *et al.* [142] reported the epitaxial growth of MnZn-ferrite films on $\mathrm{SrTiO_3}$ with and without $\mathrm{BaZrO_3}$ buffer layers.

Guyot *et al.* [143] reported the growth of Co-ferrite films, while Terzzoli *et al.* [144] reported the growth of Co-ferrite films on Si (100) substrates with a strong (111) crystal texture in spite of the formation of a native oxide layer at the substrate surface. Co-ferrite films grown on $\mathrm{SiO_2/Si(100)}$ substrates were also studied and reported by Paulsen *et al.* [145] for their magnetoelastic properties. Hu *et al.* [146], [147] demonstrated the structural tuning of magnetic anisotropy in PLD Co-ferrite films and expressed their findings in the context of cation disorder and local distortions. Similarly, Yang *et al.* [148], [149] illustrated enhanced magnetization in PLD Cu-ferrite films as a function of working gas pressure induced cation disorder.

A long sought goal of the ferrite community has been the integration of ferrite-based microwave passive devices with semiconductor systems. One path to realizing this goal is the growth of ferrites on semiconductor substrates. Oriented ferrite films deposited on semiconductor substrates are made difficult by the high temperatures required to grow a ferrite having low microwave loss. Further difficulties arise from the formation of native oxides on the substrate surface leading to a loss of epitaxy. In an example of ferrite—semiconductor integration was by Liu *et al.* [150] who reported the growth of oriented $\mathrm{Ba}M$ films on silicon substrates with an MgO buffer layer. Zhang *et al.* [68] applied rf magnetron sputtering to grow highly textured thin BaM films ($\sim$200 nm) on Pt coated Si substrates having FMR linewidths of less than 400 Oe. Meanwhile, Y. Chen *et al.* [151]

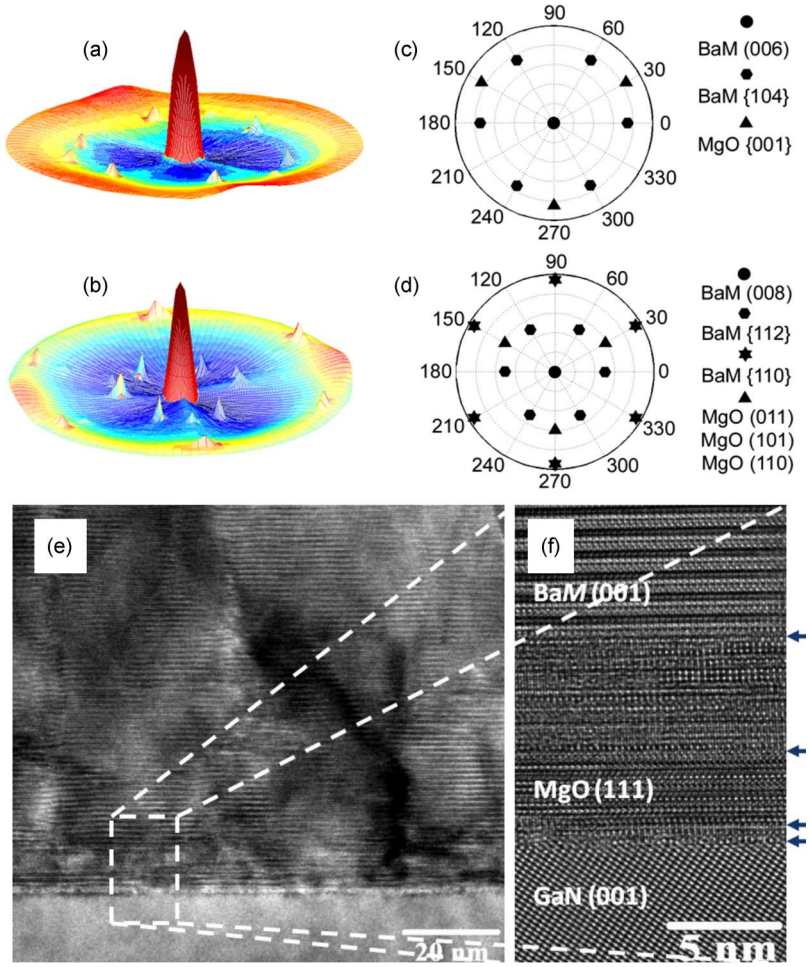

Fig. 12. Pole figures obtained for (a) the (006), and (b) (008) reflections, and the corresponding 2D projections (c) and (d), with 2θ values fixed at 23.00° and 30.30°, respectively. The single dominant peak in (a) corresponds to $\phi = \xi = 0°$ for the $\mathrm{Ba}M$ (006) reflection. The weaker peaks in (a) and (c) exhibiting six-fold symmetry correspond to closely spaced $\mathrm{Ba}M$ (104) reflections. The minor peaks exhibiting three-fold symmetry in (a) and (c) derive from closely spaced MgO (100) reflections illustrating the epitaxial nature of the $\mathrm{Ba}M$ films grown on $\mathrm{MgO/GaN/Al_2O_3}$. Similarly, (b) and (d) show similar data for the (008) reflection further supporting the epitaxial growth of films. e) Transmission electron microscopy images of the $\mathrm{Ba}M$ film grown on $\mathrm{MgO/GaN/Al_2O_3}$ in cross section. The image (f) is an expanded view of the section denoted in (e). (g) Hysteresis loops obtained by vibrating sample magnetometry (VSM) with a maximum applied field of 13,000 Oe aligned parallel (dashed) and perpendicular (solid) to the film plane. (h) Power derivative as a function of applied magnetic field in the region near the ferromagnetic resonance at 53 GHz. The linewidth measured as the peak-to-peak power derivative is 86 Oe for the as-deposited BaM film deposited on 8 nm $\mathrm{MgO(111)/GaN/Al_2O_3}$. (Adapted from [155].)

successfully screen-printed thick $\mathrm{Ba}M$ coatings ($\sim$ 200 μm) onto large area Si substrates buffered with alumina [152] and silica [152] having relatively high FMR linewidths of >2400 Oe. Z. Chen *et al.*, [153]–[155] reported the PLD growth of oriented $\mathrm{Ba}M$ thin films on 6H-SiC substrates with and without MgO buffer layers. These films were also successfully reactively ion etched into pillar arrays that significantly reduced the demagnetizing energy of the film and demonstrated a unique path towards self-biased structures of single crystal films. Although ion etching caused copious defects leading to enhanced coercivity a post-etch heat treatment was shown to not only recover the magnetic properties but in some instances to improve the film's properties over those of the as-deposited films. Z. Chen *et al.* extended these studies to include the deposition of high quality $\mathrm{Ba}M$ hexaferrites on MgO(001)/GaN(0001)/sapphire substrates. The latter studies included the growth of $\mathrm{Ba}M$ having perpendicular magnetic anisotropy and an FMR linewidth (peak-to-peak in the power derivative) of less than 90 Oe at 53 GHz. Fig. 12(a)–(d) depict pole figure analysis of the (006) and (008) reflections: All reflections have been identified to confirm sample orientation and epitaxy with respect to the substrate. In Fig. 12(e) and (f) are high-resolution transmission electron microscopy images illustrating the sharp interface between GaN/MgO. The MgO/BaM interface depicts an alloyed region in which a spinel phase has stabilized. A narrow FMR linewidth, 86 Oe at 53 GHz, is consistent with reduced hard axis coercivity. These studies represent the first successful growth of any low-loss microwave ferrite on a microwave compatible semiconductor substrate material.

Besides $\mathrm{Ba}M$, many hexaferrite materials have been deposited by PLD. Other M-type hexaferrites include strontium and lead hexaferrites ($\mathrm{Sr}M$ and $\mathrm{Pb}M$) [156]. Scandium doped $\mathrm{Ba}M$ films were deposited to control magnetic anisotropy [157], whereas cobalt and titanium co-doped $\mathrm{Ba}M$ and aluminum doped $\mathrm{Sr}M$ films were deposited for the optimization of the magneto-optical properties [158].

A variant to conventional PLD involves the sequential ablation from multiple targets to construct engineered unit cell struc-

tures with specific chemistry and valence leading to the tailoring of magnetic properties. This technique allows one to control cation distribution in the unit cell leading to the stabilization of ferrite structures having far from equilibrium properties. This technique has been referred to as alternating target laser ablation deposition or ATLAD. In recent years, ATLAD has been used by Zuo *et al.* [159]–[161], Yang *et al.* [150], and Geiler *et al.* [162] to control cation distribution within the ferrite lattices of Mn-ferrite, Cu-ferrite, BaM, and PbM hexaferrites. In the case of Mn-ferrite films, low oxygen pressure was shown to lead to a low cation inversion and large single ion anisotropy increasing $H_{\rm A}$ from $\sim$20 to $>$1000 Oe. In contrast, high oxygen pressures led to increases in cation inversion, distorting the cubic structure, breaking crystal symmetry, and stabilizing a perpendicular magnetic anisotropy field of $\sim$1000 Oe. Such properties provide these films unique potential for microwave applications at L, S, C, and X bands.

In the Cu-ferrite film system, Yang *et al.* [150] was able to redistribute Cu ions from $\sim$85% octahedral sites to $\sim$60% tetrahedral sites. This created an imbalance of spins between the A- and B-sublattices resulting in a magnetization increase of up to 65%. The properties for near *normal* Cu ferrite materials was predicted by Zuo *et al.* [163] using first principles band structure calculations. Geiler *et al.* [164] demonstrated for the first time the ability to calculate, locate, and confirm the lattice position through synchrotron radiation measurements the distribution of Mn dopant ions in BaM. This was the first convincing demonstration of cation engineering in ferrite systems.

A major advance allowing for this type research was the development of the x-ray absorption fine structure (XAFS) technique to track the element specific cation distribution and valence of principle and dopant ions. The first demonstration of XAFS to ferrites systems was Harris *et al.* [165]–[167] who applied a multiple scattering XAFS model that revealed unique signatures that identified A- and B-site lattice occupation of cations. Calvin improved upon Harris' approach by imposing a multi-absorption edge co-refinement leading to results that were more statistically robust [168]. This approach has been applied to thin films [146], [147], [149], [150], [165]–[168], [161]–[163]; particles [169] and nanoparticles [168]–[172] systems.

Limitations of PLD and ATLAD ferrite film fabrication include limited film thickness, typically $< 2{-}3\ \mu$m, and high temperature processing, typically $>$ 800°C. At these thicknesses the films are not well-suited for microwave device applications, while growth at these high temperatures is incompatible with semiconductor device fabrication. As a result, PLD remains a valuable research tool but does not adequately address the materials needs of the microwave device community. During the last decade, Abe and co-workers [173], [174] have developed a wet chemistry deposition technique, i.e., spin spray ferrite plating, which allows low temperature processing of thick ferrite films. We next discuss the advantages and disadvantages of this technique.

B. Spin Spray Ferrite Plating

In spin spray plating (SSP) the nucleation and growth of a solid phase film is facilitated by hydrolysis without pyrolysis. Abe *et al.* first began developing SSP during the mid-1980s as a means of processing ferrite films at low temperatures [173]. Abe provided a thorough review of the science and technology of SSP in 2000 [174]. The advantages of SSP include rapid growth rates, thick dense films, low temperature processing, and a wide range of suitable substrate materials that range from plastics to ceramics. This technique involves the spraying of metal acid solutions, commonly metal chloride solutions, and oxidizing agents, commonly sodium nitrite solutions, via nebulizers onto rotating substrate materials held at temperatures ranging from room temperature to 90°C. In this deposition scheme, one can produce polycrystalline films having the spinel structure ($(\mathrm{M,Fe})_3\mathrm{O}_4$, M = Fe, Co, Ni, Zn, Mn, etc.) directly from an aqueous solution. This technique has been extended to the deposition of ferrites onto a variety of substrates including rolls of plastic sheet [175]. Requiring no post-deposition heat treatments, SSP allows the deposition of ferrite films on such non-heat-resistant materials as semiconductor substrates [176] and polymer sheets [177] for EMI suppression and other purposes.

NiZn-ferrite noise suppressors have been demonstrated to absorb noise currents by magnetic losses as they radiate. In using SSP one can deposite ferrite films onto polyimide sheets that are cut and pasted onto noise sources or deposite films directly onto printed circuit boards, covering potential noise sources [178].

SSP NiZn ferrite films, 3 μm in thickness, suppress GHz noise more effectively than commercialized noise suppressors. The sheet type noise suppressors, made by a roll spray ferrite plating process, have surface resistivities higher than $1 \times 10^5\ \Omega - \mathrm{cm}^2$, stability to temperatures greater than 260°C (i.e., the lead-free soldering temperature) [178], and the ability to withstand the standard bend test (JIS C5016: no peel off occurred after one million cycles of bending at a 3 mm radius of curvature) [179]. Spin sprayed NiZnCo ferrite films have been shown to have natural resonance frequencies from 3 to 5 GHz and values of μ' from 5 to 8 at frequencies up to a few GHz. These films are promising for magnetic field shielding for 900 MHz RFID applications [180].

Even with thicker SSP films samples often fall short of the needs for many microwave applications. The FMR linewidths of SSP films are higher than those processed by PLD, for example, with losses attributed to contaminants from chemical processing.

In contrast to SPP, liquid phase epitaxy (LPE) is a technique that has been shown to provide thick films and near single crystal quality. We next examine the LPE growth of ferrites.

C. Liquid Phase Epitaxy of Thick Ferrite Films

In liquid phase epitaxy, oxide compounds such as ferrites are mixed and dissolved in solvents or fluxes. Common fluxes include boron oxide ($\mathrm{B_2O_3}$), barium oxide (BaO) and $\mathrm{B_2O_3}$, lead oxide (PbO), or a mixture of $\mathrm{B_2O_3}$ and PbO. In general, the composition of the flux mixtures is chosen so that the melt temperature does not exceed $\sim$ 1000°C. The substrate acts as a seed onto which the ferrite film nucleates and grows. Appropriate lattice matching is considered to minimize stress-induced crystal defects that limit film thickness and performance [181].

LPE was first employed to produce high quality yttrium iron garnet (YIG: $\mathrm{Y_3Fe_5O_{12}}$) films by Linares [181]. LPE-grown garnets continue to receive a great deal of attention for high

frequency applications such as microwave and millimeter wave devices and optical Faraday isolators [182]. Growth rates in LPE can be 10s μm/hr leading to film thicknesses up to and greater than 200 μm [183]. Rapdi growth rates is a definite advantage over other deposition techniques including physical vapor deposition or chemical vapor deposition methods. In all film deposition methods that aim to maintain epitaxy, a common difficulty is lattice mismatching between ferrite and substrate. A favored substrate for the deposition of garnets, i.e., gadolinium gallium garnet (GGG), has the common garnet crystal structure with a close match to the thermal expansion coefficient of YIG, in addition to a lattice mismatch of only 0.06% [182]. Although the lattice mismatch is exceedingly small compared to the mismatches of many semiconductor materials or oxide heterostructures, these mismatches can give rise to larges stresses that have deleterious effects upon film structure and properties. However, the LPE growth of YIG on double-sided GGG provides a cancellation of in-plane stresses that result in optimal film thicknesses in excess of 200 μm. These films have been measured to have FMR linewidths of less than 1 Oe at ~9 GHz [182]. A number of spinel ferrites have been grown by LPE [184], but crystal quality and thickness have yet to reach the level of LPE garnets. LPE grown hexagonal ferrites, especially barium hexaferrite, have received great attention [185]. The smallest linewidth obtained for LPE grown epitaxial barium hexaferrite on single crystal hexagallate, i.e., $SrGa_{12}O_{19}$, substrates was ~27 Oe at 60 GHz [186]. These values are compared with $\Delta H < 10$ Oe for the best barium hexaferrite single crystal sphere [187] and a value of ~10 Oe predicted for Mn-doped hexagonal ferrite [188]. Hexagonal ferrite films having the c-axis perpendicular to the substrate plane have been grown by LPE on PLD grown seed layers on commercially available substrates [189]–[191]. A ΔH value, 28 Oe, was measured from a 45 μm film grown on double-sided (111) MgO [191]. Alternatively, a 200 μm BaM film with the c-axis aligned along the in-plane direction, grown on double-sided m-plane Al_2O_3 had a ΔH of 70 Oe at 60 GHz [189].

The LPE technique has clear advantages over other physical and chemical deposition techniques, producing films of thickness > 200 μm having high crystal quality that in some cases approaches that of single crystals. These films are very well suited for microwave and millimeter wave devices that require low-losses. However, they continue to require a biasing magnet to saturate the film thus adding size, weight, and assembly cost. We next examine a second technique that provides film thicknesses in the 100s μm but has until recently been limited by poor crystalline quality and high microwave losses [87].

D. Screen Printed Coatings

In general, thick films can be achieved by physical processes such as tape casting, screen printing, and LPE, among other techniques. Due to simplicity and cost-effectiveness, screen printing has been extensively used in mass production of multilayer chip inductors, transformers, ceramic thick film circuits, and magnetic sensors and actuators [192].

It is predicted that next generation microwave devices will be planar, self-biased, low-loss and integratable with semiconductor systems. Self-biasing is an important property that eliminates the need for permanent bias magnets thus reduces size, weight, and cost of microwave devices, components and systems [193]. In addition to high remanent magnetization and low microwave losses, thicknesses of > 100 μm are sought.

Yuan *et al.* [194] reported screen printed SrM films on alumina substrates by hydrothermal synthesis. That work detailed influences of precurser powders and sintering processes on static magnetic properties. Because thicknesses ranged from 8 to 15 μm and possessed low values of hysteresis loop squareness (M_r/M_s), i.e., 77%, these films failed to meet the materials needs of self-biased microwave electronic devices.

Y. Chen *et al.* demonstrated BaM thick films (100 ~ 500 μm) prepared by screen printing followed by sintering heat treatments [195], [196]. Structural, magnetic and microwave measurements confirmed that the polycrystalline films were suitable for applications in self-biased microwave devices in that they exhibited a large remanence, $4\pi M_r = 3800$ G, high hysteresis loop squareness, 96%, and relatively low microwave loss (derivative linewidths of ~310 Oe at 55.6 GHz). Among mechanisms contributing to the losses, an extrinsic linewidth broadening, $\Delta H_{ex} = 274$ Oe, was dominant. This linewidth arose from pores and the misalignment of grains. Subsequently, a narrower linewidth, $\Delta H = 212$ Oe at 53.5 GHz, was measured for screen printed thick films by including a hot-press sintering step [184]. Fig. 13(a) shows a scanning electron microscopy (SEM) image with the cross-section as Fig. 13(b) of the BaM film 250 μm in thickness. Fig. 13(c) is a plot of hysteresis loops illustrating the high remanent magnetization providing self-bias properties. Although the films still contains pores and misaligned grains, the results have demonstrated that the screen printing technique is capable of processing thick, self-biased, low-loss BaM films; an integral step in the processing of planar microwave magnetic devices [87].

E. Quasi Single Crystal and Crystallographically Textured Compacts

In the 1950s, single crystal ferrites were routinely processed and studied for their magnetic and microwave properties. The literature is replete with such references and therefore we direct the reader to reviews of ferrite materials targeting this timeframe [17], [21], [197].

There is still a great need for single crystal and quasi-single crystal ferrites. Such materials possess among the lowest FMR linewidths and therefore are ideal for microwave devices in which ultralow-losses (and high Q) are required. In this section we address recent developments in the growth of high quality compacts, quasi-single crystal compacts, and crystallographically textured compacts with emphasis placed on the prototypical and versatile hexaferrites.

Although single crystal ferrites remain widely used as resonators, aspects of single crystal growth that limit their wide utility include: the inability to grow large numbers of large crystals; the inability to grow crystals having exotic compositions and structures; and, the inability to grow crystals having the appropriate aspect ratio for low dimensional planar device topologies.

Since the 1980s, the study of ferrites as single crystals have largely been confined to thin epitaxial films processed by PLD (as previously discussed), thick (quasi) single crystal ferrite

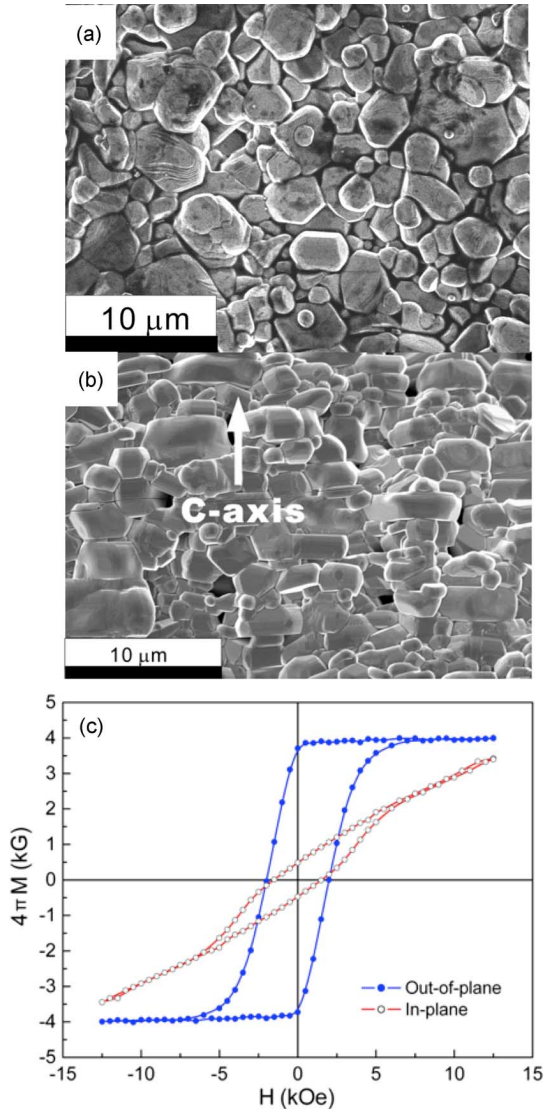

Fig. 13. Scanning electron microscopy images of a 200 μm screen printed film after alignment and heat treatment procedures: (a) surface and (b) cross-section. Magnetic hysteresis loops acquired with the applied magnetic field aligned along the in-plane sample direction (open squares) and perpendicular to the sample plane (solid squares). (Adapted from [66].)

films processed by LPE (as previously discussed), and as single crystal nano-, micro-, or mesoscale particles [198]–[205]. A recent article on the topic of magnetic particles by Willard *et al.* [16], provides a complete review of magnetic particles, including ferrites, prepared by chemical means. Since these small particles (i.e., with diameters less than the single magnetic domain) lack grain boundaries and misoriented grains, they are typically studied to elucidate fundamental properties of ferrites or in exploring dc magnetic properties of nanostructures as opposed to functional high frequency device applications. However, small ferrite particles have found utility as microwave absorbers [206].

Demands for improved microwave device performance and recent novel materials and devices, such as ferrite-based negative index metamaterials (NIMs) and NIMtronic devices that require ultralow-loss ferrite crystals, the need for such quasi-single crystal materials has returned. The role of ferrites in metamaterial heterostructures have been discussed.

As has been discussed earlier, garnets and spinel crystals and compacts can operate under bias magnetic fields up to Ku frequencies, respectively. Sc or In doped $\mathrm{Ba}M$ or $\mathrm{Sr}M$ hexaferrites are considered for $f < 40$ GHz due to their relatively low FMR frequencies. For example, $\mathrm{BaFe_{11}ScO_{19}}$ ferrite, prepared by conventional ceramic processing, demonstrated a magnetization squareness of 83% and anisotropy fields of less than 10 kOe. The X-band FMR derivative linewidth was measured to be more than 800 Oe. For devices which operate at $f > 40$ GHz, $\mathrm{Ba}M$-type hexaferrites are available. When doped with Al or Ga the FMR is shifted to higher frequencies and these materials may be used up to and beyond W-band [33].

Most recently, low microwave losses and high squareness of the hexagonal Sc-doped Ba ferrites, having also low magnetocrystalline anisotropy fields ($\mathrm{H_A}$ = 4–10 kOe), have been successfully achieved. Y. Chen *et al.* made use of a polymer network-assisted alignment processing (PNAAP) technique to effectively align hexaferrite particles in high magnetic fields to realize a highly dense oriented Sc-doped Ba ferrite compact [207]. A 2-step heat treatment of the resulting compact lead to FMR linewidths of ∼500 Oe at X-band and Ka-band and high magnetization squareness, $\mathrm{M_r/M_s} \sim 92\%$. These materials have unique potential for use in self-biased microwave and millimeter devices at frequencies from 10–40 GHz.

High crystal texture in $\mathrm{Ba}M$ compacts were also realized when nanorods of goethite, i.e., α-FeOOH, were mixed with $\mathrm{BaCO_3}$, dispersed in a polymer solution, and oriented under a high (∼90 kOe) magnetic field during polymerization [208]. The orientation arose principally from the interaction of the magnetic field with the anisotropic antiferromagnetic goethite particles. The oriented antiferromagnetic particles acted as seeds for the topochemical growth of $\mathrm{BaFe_{12}O_{19}}$ ferrite grains along the [0001] direction. The degree of grain orientation was determined using magnetic measurements and orientation distribution functions and pole figures determined by electron backscatter diffraction analysis (EBSD, see Fig. 14(a)). In Fig. 14(a), the color red signifies the out of plane orientation of the hexaferrite crystallographic c-axes. This is further illustrated by the pole figure of Fig. 14(b) in which the (0001) reflection is seen as a well-focused peak in the figure signifies the high degree of crystal orientation. Finally, in Fig. 14(c) one sees the clear and unambigious anisotropy in magnetic properties. The inset shows a scanning electron microscopy (SEM) image of large, oriented, and coalesced grains.

In addition to the hexaferrite compacts for self-biased microwave devices, a quasi-single crystal (QSC) Sc-doped $\mathrm{BaFe_{12}O_{19}}$ ferrite has attracted interest from the microwave engineering community [209]. The material was fabricated by a single solid-state reaction technique that included the alignment of the ferrite seed crystals. This technique was shown to be cost-effective in producing future microwave devices compared with those that employ $\mathrm{Ba}M$ single crystals. Fig. 15(a)–(c) depict an SEM image illustrating a collection of large, coalesced crystals having strong c-axes alignment out of the sample plane (see Fig. 15(b)). The QSC ferrite bulk samples show similar static magnetic properties to those of single crystals (see Fig. 15(c)). However, it's FMR linewidths are ∼300 Oe

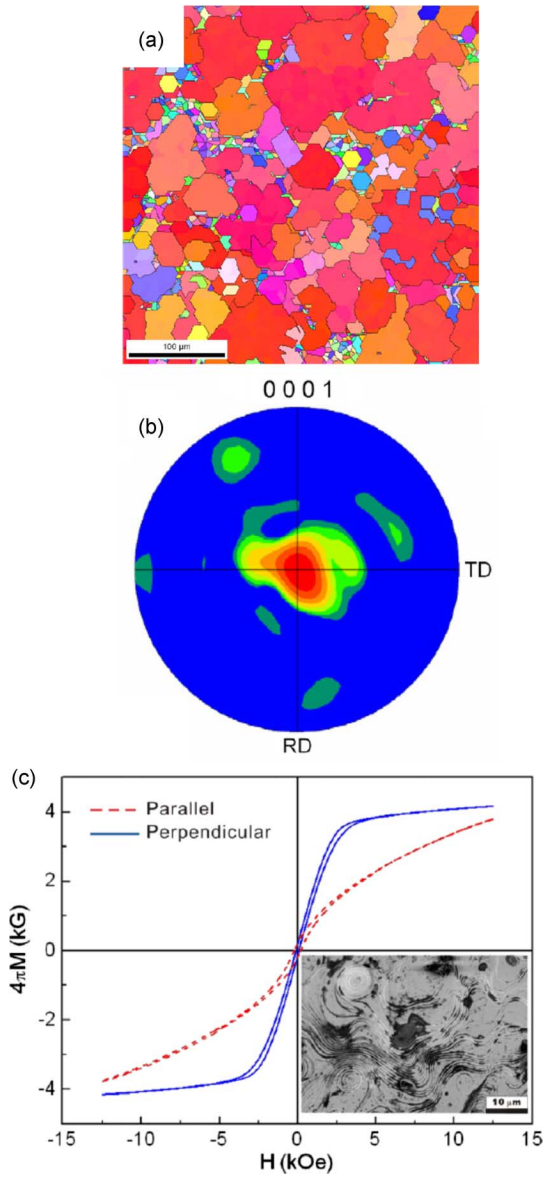

Fig. 14. a) Orientation map along the [0001] direction measured by EBSD for the BaM ferrite sintered by the topochemical growth process. The color code for the crystallographic orientations is given in the stereographic triangle below the map. b) Pole figure along the [0001] direction for the BaM ferrite sintered by the topochemical growth process. c) Magnetic hysteresis loops and SEM image of the surface morphology for the BaM compact sintered at 1350°C for 10 hours. Perpendicular and parallel refer to the orientation of the applied magnetic field with respect to the sample surface. (Adapted from [208].)

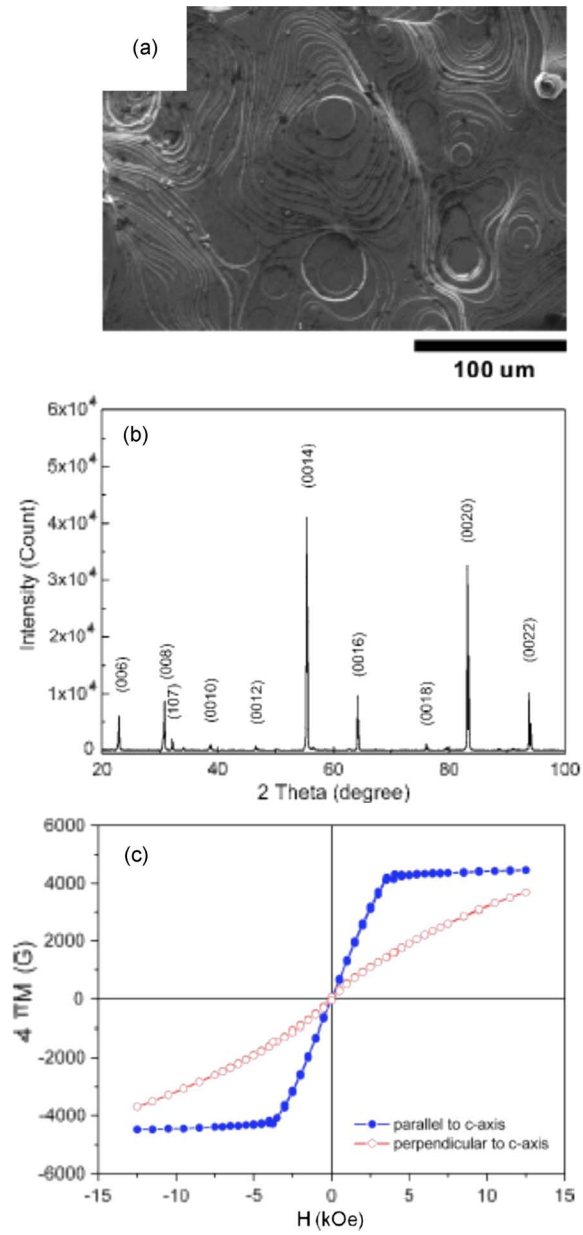

Fig. 15. a) SEM micrograph for the surface of a $\mathrm{Ba}M$ ferrite quasi-single-crystal. b) X-ray diffraction pattern of a $\mathrm{BaFe_{12}O_{19}}$ $\mathrm{Ba}M$ quasi-single-crystal. c) Hystersis loops of Ba ferrite quasi-single-crystal when an external field is parallel and perpendicular to the c axis. (Adapted from [209]).

at U-band frequencies, broader than Ba ferrite single crystals, $<$100 Oe. Nevertheless, a 300 Oe linewidth is acceptable for many microwave and millimeter wave device applications.

Z-type hexaferrite single crystals like the Y-type, and unlike the M-type, have their easy magnetic direction aligned with six-fold symmetry within the basal plane (a–b plane). Efforts to crystallographically orient such grains must apply magnetic fields in the plane of the compact, typically isotropically within the plane. Daigle *et al.* accomplished such in orienting of $\mathrm{Co_2Z}$ type particles by first forming $\mathrm{Co_2Z}$ hexaferrite through a modified aqueous co-precipitation of elements method [210]. Powders were mechanically pressed into compacts using uniaxial pressure followed by sintering at 1250°C for 10 hours in oxygen. After sintering, compacts were crushed and the powder was reduced to a single domain particle size (1–2 μm). Phase purity of the samples was verified with x-ray diffraction (XRD) measurements. A representative $\theta - 2\theta$ spectrum collected using Cu kα radiation is shown in Fig. 16(a). A typical hysteresis loop of loose $\mathrm{Co_2Z}$ hexaferrite powder is shown in Fig. 16(b). Saturation moment of as prepared ferrite powder (assuming bulk density) was measured to be 3310 G, in good agreement with bulk reference data of 3350 G [211]. Scanning electron microscopy (SEM) images of the sintered ferrite powder are shown in Fig. 16(c) and (d). Large hexagonal grains with diameters of up to 20 μm are visible in the SEM images. After attrition, single magnetic domain particles were oriented using a rotating magnetic field in the plane of the

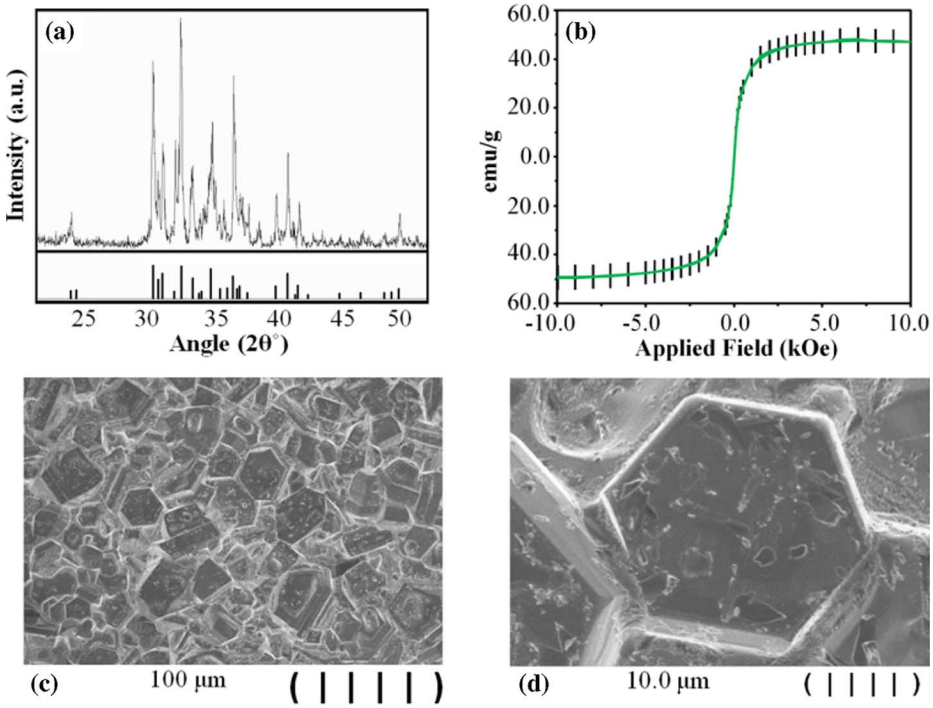

Fig. 16 (a) X-ray diffraction spectrum of sintered Co_2Z hexaferrite powder compared with reference JCPDS file no. 19-0097. (b) Room temperature magnetic hysteresis loop of Co_2Z hexaferrite powder. (c) and (d) SEM images of Co_2Z hexaferrite powder at different magnifications.

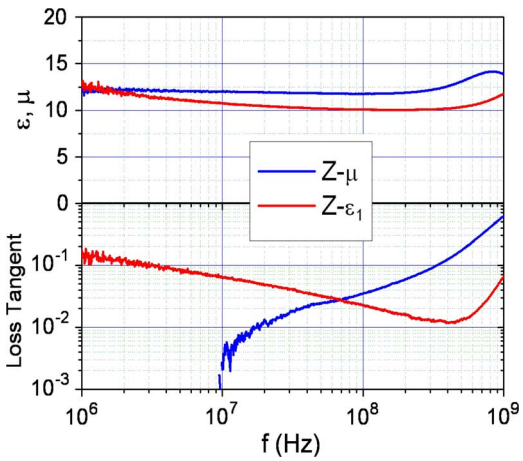

Fig. 17. (a) Permittivity and permeability spectra (linear scale) as well as (b) loss tangents (logarithmic scale) of Co_2Z hexaferrite materials created for EBG metamaterial applications.

compact. The goal of the magnetic orientation process was to align the anisotropic ferrite particles with their crystallographic c-axes perpendicular to the compact plane to maximize the permeability [212], [213]. Typical spectra of the complex permeability and permittivity of samples was measured from 1 MHz to 1 GHz for magnetically oriented samples are shown in Fig. 17. Real part of the permeability was measured to be approximately 14 while the real part of permittivity was measured to be 10. These values are in good agreement with those in previously published works [214]. For isotropic samples, the real part of the permittivity and permeability was measured to be 14 and 7, respectively, confirming the utility of the magnetic field orientation method in enhancing the permeability of hexaferrite compacts. These materials were prepared as possible electromagnetic bandgap substrates for antenna elements in an effort to reduce the antenna profile [215].

F. Ferrites Exhibiting the Magnetoelectric Effect

The magnetoelectric (ME) effect, first predicted in 1894 [216], described theoretically in 1959 [217], and observed experimentally in 1960 [218], has attracted much attention because of its unique potential for the development of novel ME devices. The ME effect observed in the vast majority of single phase materials is weak and typically observed only under the application of strong magnetic fields and at low temperatures [219]. Some of the more significant requirements for realizing practical devices based on ME materials include good insulating properties and magnetic ordering above room temperature [220]. Both of these requirements are satisfied in ferrite materials, and indeed, several members of this magnetic oxide family have exhibited the ME effect near room temperature. This effect, however, has been shown to be too weak at low magnetic fields to meet the needs of practical devices. The observation of a strong ME effect in rare-earth based magnetic oxides, such as $TbMnO_3$ [221], suggest the possibility of a strong coupling between magnetization and electric polarization in long-wavelength magnetic structures (e.g., spiral or helical spin structures. With the recent discovery of large ME effect in transition metal oxides [220], considerable effort has been devoted to the study of magnetically frustrated systems having long-period magnetic structures. These advances provide promise in the simultaneous manipulation of both permittivity and permeability enhancing the dynamic response in spatial, temporal, and frequency domains. In 2005, Kimura, Lawes, and

Ramirez demonstrated the control of electric polarization (P) by applying magnetic field (B) to a hexaferrite crystal having magnetic order above room temperature [220]. The material investigated was a hexagonal Y-type $Ba_{0.5}Sr_{1.5}Zn_2Fe_{12}O_{22}$, which is a non-ferroelectric helimagnetic insulator in its ground state. The helical spin structure of $Ba_{0.5}Sr_{1.5}Zn_2Fe_{12}O_{22}$ can be modulated by the application of a magnetic field perpendicular to the crystallographic c-axis. By increasing the magnitude of B from 0 to 2.2 T, the system undergoes successive magnetic transitions, and shows concomitant ferroelectric order in some of the induced phases. The strong interplay of electric and magnetic polarizations observed in $Ba_{0.5}Sr_{1.5}Zn_2Fe_{12}O_{22}$ provides unique opportunities for applications employing hexaferrites having structures related to magnetoplumbite (e. g. $BaFe_{12}O_{19}$), which has long been used as a permanent magnet [222] a magnetic recording media [67], and as a key component in rf, microwave, and millimeter-wave devices [87]. In 2008, Ishiwata, Taguchi, Murakawa, *et al.* [223] demonstrated low magnetic field control of the electric polarization in a helical $Ba_2Mg_2Fe_{12}O_{22}$ single crystal hexaferrite. Both the magnitude and the direction of P in this longitudinal helimagnet were controlled by manipulating the spin cone axis with small B ($\sim$ 0.03 T). Similar to the $Ba_{0.5}Sr_{1.5}Zn_2Fe_{12}O_{22}$ system, $Ba_2Mg_2Fe_{12}O_{22}$ undergoes several magnetic transitions with a maximum P of $\sim 80\ \mu C/m^2$ measured at 5 K ($B = 0.2$ T). As recently as 2010, Kitagawa, Hiraoka, Honda, *et al.* [224] demonstrated the manipulation of P with low B (<0.25 T) at room temperature in a polycrystalline Z-type hexaferrite. The variation in P with B for the ceramic sample with the composition $Sr_3Co_2Fe_{24}O_{41}$ is shown in Fig. 18. These findings show the ability of this system to store information as polarized spin helixes as binary digits. As such, Z-type hexaferrites exhibiting room temperature ME effect may be suitable for the development of ME devices, including non-volatile memory.

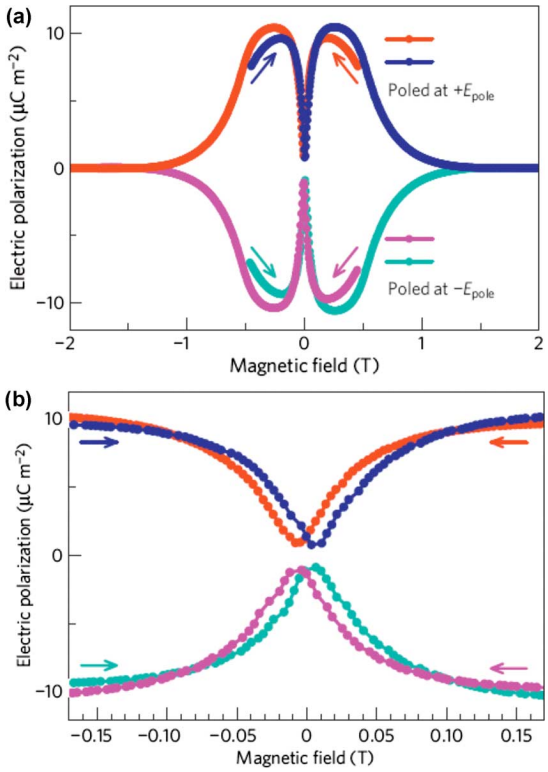

Fig. 18. Room temperature magnetoelectric effect in $Sr_3Co_2Fe_{24}O_{41}$ polycrystalline ceramics sintered in oxygen. (a) Magnetic field dependence of electric polarization for -2 to $+2$ T and (b) expanded view of the same data from -0.17 to 0.17 T. (Adapted from [224]).

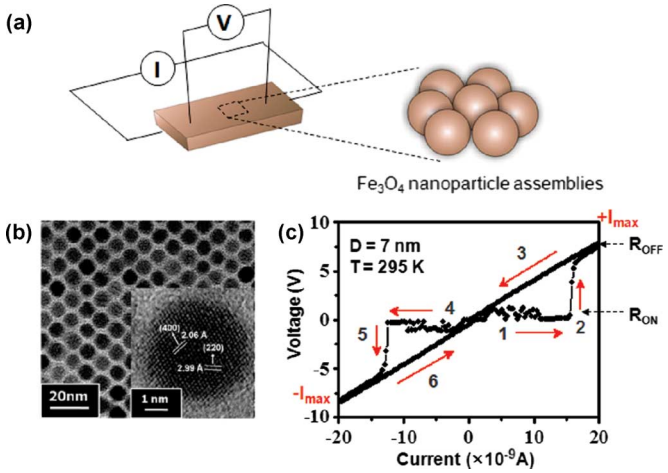

Fig. 19. Nanoparticle assemblies (a) of consisting of an infinite number of monodispersed crystalline magnetite (Fe_3O_4) particles below 10 nm (b) exhibit room temperature a voltage-current hysteresis with an abrupt and large bipolar resistance switching ($R_{OFF}/R_{ON} \approx 20$) (c). (Adapted from [228]).

G. Ferrite Nanostructures as Memristors

In 1971, Leon Chua [225] conjectured from symmetry arguments that a fourth fundamental passive circuit element in addition to the capacitor, inductor, and resistor should exist. He named this 4th element the memristor, short for memory resistor. Among the many potential properties and applications included ultrahigh density two terminal electronic resistance switches. In 2008, Strukov *et al.* [226] showed that memristors naturally evolve in nanoscale systems where electronic and ionic transport couple under the application of an electric field. Although their findings extend to many nanosystems, they most effectively demonstrated the effect in $Pt/TiO_2/Pt$ heterostructures. J.J. Yang *et al.*, also in 2008 [227], demonstrated a nonvolatile memristor memory cell that stores information in bistable conductance states. The devices are fast, small and scalable, and compatible with CMOS processing protocols providing unique potential as a future static or dynamic memory technology. Kim *et al.* [228] in 2009 demonstrated the effect in nanoparticle assemblies (see Fig. 19(a), (b)) of Fe_3O_4 and other spinel ferrites. In that work, assemblies of particles having average sizes less than 10 nm exhibited room temperature i-v hysteresis illustrating an abrupt bistable resistance switching. The bistable i-v characteristics observed illustrate that the switching properties are related to the hysteresis behavior as the current is swept through steps 1–6 of Fig. 19(c). No damage or breakdown was experienced upon repeated cycles. In this same publication studies were performed on Mn-ferrite revealing a similar memresitor effect albeit at lower temperatures. Other examples of dynamic control of i-v properties by both electric and magnetic fields have been measured in polycrystalline MnZn-ferrite ceramic compacts [229]. In related studies, Y. Chen *et al.*, [230] demonstrated the tunability of permittivity

by the application of magnetic field. This latter study was communicated as a magnetodielectric effect but is closely related to the above phenomenon.

H. The Role of Ferrites in Tunable Negative Index Metamaterials

Recent advances in metamaterials possessing negative index of refraction (NIM) and strong dispersion characteristics has allowed for the development of novel microwave technologies [108]. A significant recent development is the fabrication of tunable negative index metamaterials utilizing high quality ferrite materials [109]–[113]. The tunability and low-losses observed in ferrite-based NIMs make them ideal constructs for designing tunable, broadband, compact and light weight microwave and mm-wave devices. In ferrite TNIMs a change in permeability by the application of magnetic field causes a change in the phase velocity of the microwave signal traveling through the TNIM. Experimental and theoretical investigations of field tunable negative refractive index metamaterial (NIM) using a yttrium iron garnet (YIG) films and an array of copper wires in waveguides were carried out by both P. He *et al.* and Y. He, *et al.*: A key feature of magnetic field tunability of the NIM in the microwave frequency region was demonstrated [109]–[113]. Transmission passbands were realized in the negative refractive index region that could be tuned by an external magnetic field. The permeability of the NIM was simultaneously tuned along with the refractive index. The change in permeability or refractive index leads to a change in the phase velocity of the signal and, therefore, the phase of the transmission coefficient. Such an effect can be readily employed to realize TNIM phase shifters [111], [112]. The advantage of using a ferrite NIM for phase shifter applications is that it allows for low-loss operation over frequencies near FMR where μ' is negative and relatively high. This was presented and discussed in greater detail in Section IV-C. In the field tunable NIM, the effect of the ferrite is to provide a tunable negative permeability over a continuous range of frequencies on the high frequency side of FMR.

Complementary negative permittivity, ε', can be achieved using a single periodic array of copper thin film wires deposited on Kapton. A negative refractive index region of 0.5 GHz in width at K band was demonstrated by P. He [111]. Increasing the volume of the YIG increased the absorption and therefore a tradeoff between bandwidth for the negative index region and low-loss was realized. Additionally, the dielectric permittivity of the YIG slabs reduced the effective negative permittivity obtained from the plasmonic copper wires. A similarly structured tunable negative index metamaterial was designed, fabricated and tested in a Q-band rectangular waveguide [113]. The structure consisted of a single crystalline scandium-doped barium hexaferrite $(\mathrm{Sc}-\mathrm{Ba}M)$, aligned parallel to two rows of periodic copper wires. The magnetic field tunable passband was measured indicating the occurrence of the negative refractive index.

These examples of TNIM-based electronic components represent a new approach in the design and fabrication of miniature microwave passive devices that rely upon tuning the permeability spectrum in frequency space near FMR in a NIM. Although presently they remain in the conceptual phase, these novel approaches provide unique opportunities and pathways to realizing new ferrite-based microwave technologies.

VI. Outlook

Modern ferrites have been studied since the 1930s and their application in microwave device technology dates to the 1950s. For this reason ferrites are considered a mature technology with the implication being that anticipated advances will be incremental. This in fact is far from reality. Advances in materials processing and devices taking place during the last ten years have been dramatic and significant.

Alternating target laser ablation deposition has been shown to allow control of cation distribution within a unit cell providing opportunities to fabricate far from equilibrium structures and ultimately to tailor magnetic, electronic, and microwave properties for specific applications. Screen printing has been shown to be an effective tool in the processing of thick, self-biased, and low-loss ferrite films for cost effective processing of next generation self-biased planar ferrites. This breakthrough could prove to be a disruptive advance in monolithic microwave integrated circuits technology. Still, when nothing less than single crystal quality, low-loss, high Q ferrites, are needed, LPE and QSC compacts provide ultra-low FMR linewidths.

In addition to materials advances, we find that new devices having enhanced performance, reduced size, and in some instances added functionality, have been realized. The ability to process thick film ferrites having perpendicular magnetic anisotropy and self-bias properties allows for the redesign of conventional microwave passives as light weight planar constructs. Likewise, low temperature processing of ferrite coatings by SSP on plastics allow now for improved EMI suppression. New devices, based upon spin wave parametric pumping and nonlinear spin waves in feedback rings, employ ferrite films for high frequency signal processing [231], [232]. Finally, NIM constructs employing low-loss ferrites, allow for a new class of tunable microwave electronics that are small in size, profile, and weight and offer broadband active tuning.

In lieu of these advances, it appears that the microwave materials and device technologies are in a state of significant positive change with the potential to greatly impact a wide range of technologies that send, receive, and manipulate electromagnetic signals.

Acknowledgment

Throughout my career as a scientist, engineer, educator, and entrepreneur, I have been blessed and humbled by the unselfish mentorship of leading scientists, the support and friendship of hundreds of highly skilled colleagues and collaborators, inspiration gained from dozens of hard working and dedicated students, and the overwhelming support of family. I am particularly indebted to Prof. Carmine Vittoria, and Drs. Tim Elam, Norman Koon, and Kristl Hathaway, who all played major and unselfish roles in assisting me in all aspects of my career. I thank my wife and partner, Linda Hsu-Harris, and daughter Bailey and son Conor for there unwavering support.

REFERENCES

[1] D. Song and G. Li, *History of Electromagnetism: Observation and Utilization of Electrical and Magnetic Phenomena*. Guang Xi, China: Popular Press, 1987.

[2] M. Brand, S. Neaves, and E. Smith, "Lodestone," Museum of Electricity and Magnetism, Mag Lab U US National High Magnetic Field Laboratory, retrieved 2009-06-21, 1995.

[3] J. F. Keithley, *The Story of Electrical and Magnetic Measurements: From 500 B.C. to the 1940s*. New York: Wiley-IEEE Press, 1999.

[4] S. Li, "Origine de la Boussole 11. Aimant et Boussole," *Isis*, vol. 45, no. 2, pp. 175–196, Jul. 1954.

[5] J. Needham, *Physics and Physical Technology, Part 1, Physics, Science and Civilization in China*. Taipei, Taiwan: Caves Books, 1986, vol. 4.

[6] J. L. Snoek, "Magnetic and electrical properties of the binary system MO Fe_2O_3," *Physica*, vol. 3, p. 463, 1936.

[7] J. L. Snoek, "Non-metallic magnetic material for high frequencies," *Philips Tech. Rev.*, vol. 8, p. 353, 1946.

[8] H. A. Kramers, "L'interaction entre les atomes magnétogènes dans un cristal paramagnétique," *Physica*, vol. 1, p. 182, 1934.

[9] P. W. Anderson, "Antiferromagnetism. Theory of superexchange interaction," *Phys. Rev.*, vol. 79, no. 2, pp. 350–356, 1950.

[10] J. H. Van Vleck, "Recent developments in the theory of antiferromagnetism," *J. Phys. Radium*, vol. 12, no. 3, p. 262, Mar. 1951.

[11] L. Néel, *Annales de Physique, Paris* vol. 3, p. 137, 1948.

[12] R. H. Kodama, A. E. Berkowitz, E. K. McNiff, and S. Foner, "Surface spin disorder in $NiFe_2O_4$ nanoparticles," *Phys. Rev. Lett.*, vol. 77, pp. 394–397, 1996.

[13] Y. Yafet and C. Kittel, "Antiferromagnetic arrangements in ferrites," *Phys. Rev.*, vol. 87, pp. 290–294, 1952.

[14] R. Swaminathan, M. E. McHenry, P. Poddar, and H. Srikanth, "Magnetic properties of polydisperse and monodisperse NiZn ferrite nanoparticles interpreted in a surface structure model," *J. Appl. Phys.*, vol. 97, p. 10G104, 2005.

[15] S. Son, R. Swaminathan, and M. E. McHenry, "Structure and magnetic properties of thermally plasma synthesized Mn and Mn-Zn ferrite nanoparticles," *J. Appl. Phys.*, vol. 93, pp. 7495–7497, 2003.

[16] M. A. Willard, L. K. Kurihara, E. E. Carpenter, S. Calvin, and V. G. Harris, "Chemically prepared magnetic nanoparticles," *Int. Mater. Rev.*, vol. 49, no. 3–4, p. 125, 2004.

[17] J. Smit and H. P. J. Wijn, *Ferrites*. New York: Wiley, 1959, p. 149.

[18] J. Smit and H. P. J. Wijn, *Ferrites*. New York: Wiley, 1959, p. 157.

[19] J. Smit and H. P. J. Wijn, *Ferrites*. New York: Wiley, 1959, p. 157.

[20] J. Smit and H. P. J. Wijn, *Ferrites*. New York: Wiley, 1959, p. 174.

[21] W. H. von Aulock, *Handbook of Microwave Ferrite Materials*. New York: Academic Press, 1965.

[22] H. S. Yoder and M. L. Keith, "Complete substitution of aluminum for silicon: The system $3MnO \bullet Al_2O_3 \bullet 3SiO_2 - 3Y_2O_3 \bullet 5Al_2O_3$," *Amer. Min.*, vol. 36, p. 519, 1951.

[23] F. Bertaut and F. Forrat, "Structure of ferrimagnetic rare-earth ferrites," (in French.) *Compt. Rend. Acad. Sci.*, vol. 242, p. 382, 1956.

[24] E. G. LeCraw, E. G. Spencer, and C. S. Porter, "Ferromagnetic resonance line widths in yttrium iron garnet single crystals," *Phys. Rev.*, vol. 110, no. 6, pp. 1311–1313, Jun. 1958.

[25] J. Smit and H. P. J. Wijn, *Ferrites*. New York: Wiley, 1959, p. 191.

[26] G. R. Harrison and L. R. Hodges, Jr., "Microwave properties of polycrystalline hybrid garnets," *J. Amer. Ceram. Soc.*, vol. 44, p. 214, 1961.

[27] A. Vassiliev, J. Nicolas, and M. Hildebrant, "Sur les Proprieties des Grenats Mixtes Yttrium-Gadolinium," *Comp. Rend.*, vol. 252, p. 2529, 1961.

[28] G. Goldring, M. Schieber, and Z. Vager, "On the incorporation of neodymium in mixed yttrium-neodymium-iron garnets," *J. Appl. Phys.*, vol. 31, p. 2057, 1960.

[29] W. H. von Aulock, *Handbook of Microwave Ferrite Materials*. New York: Academic Press, 1965.

[30] J. Smit and H. P. J. Wijn, *Ferrites*. New York: Wiley, 1959, pp. 204–206.

[31] G. Albanese, A. Deriu, E. Lucchini, and G. Slokar, "Mössbauer investigation of In and Sc substituted barium hexaferrite," *Appl. Phys. A*, vol. 26, pp. 45–50, 1981.

[32] T. M. Perekalina, M. A. Vinnik, R. I. Zvereva, and A. D. Shchurova, "Magnetic properties of hexagonal ferrites with weak exchange coupling between sublattices," *Sov. J. Exp. Theor. Phys.*, vol. 32, p. 813, 1971.

[33] G. Albanese and A. Deriu, "Magnetic properties of Al, Ga, Sc, in substituted barium ferrits: A comparative analysis," *Ceramargia Int.*, vol. 5, no. 1, pp. 3–10, Jan.–Mar. 1979.

[34] L. G. Van Uitert and F. W. Swanekamp, "Permanent magnet oxides containing divalent metal ions. 11," *J. Appl. Phys.*, vol. 28, pp. 482–485, Apr. 1957.

[35] A. H. Mones and E. J. Banks, "Cation substitutions in $BaFe_{12}O_{19}$," *Phys. Chem. Solids*, vol. 4, no. 3, p. 217, 1958.

[36] K. Haneda and H. Kojima, "Intrinsic coercivity of substituted $BaFe_{12}O_{19}$," *Jpn. J. Appl. Phys.*, vol. 12, no. 3, p. 355, 1973.

[37] J. J. Went, G. W. Rathenau, and E. W. Gorter *et al.*, "Ferroxdure, a class of new permanent magnet materials," *Philips Techn. Rev.*, vol. 13, p. 194, 1952.

[38] F. Bertaut, A. Deschamps, R. Pauthenet, and S. Pickart, "Substitution dans les hexaferrites de l'ion Fe^{3+} par Al^{3+}, Ga^{3+}, Cr^{3+}," *J. Phys. Radium*, vol. 20, no. 2–3, pp. 404–408, 1959.

[39] J. Smit and H. P. J. Wijn, *Ferrites*. New York: Wiley, 1959, vol. 191, p. 204.

[40] J. Smit and H. P. J. Wijn, *Ferrites*. New York: Wiley, 1959, vol. 191, p. 210.

[41] P. Weiss, "L'hypothèse du champ moléculaire et la propriété ferromagnétique," *J. Phys. Theor. Appl.*, vol. 6, no. 1, p. 661, 1907.

[42] P. Langevin, "Magnetism and the Theory of the Electron," *Ann. Chim. Phys.*, 1905.

[43] G. F. Dionne, *Magnetic Oxides*. New York: Springer, 2009.

[44] J. Hubbard, "Electron correlations in narrow energy bands," *Proc. Roy. Soc. London*, vol. A 276, no. 1365, pp. 238–257, Nov. 1963.

[45] P. W. Anderson, "New approach to the theory of superexchange interactions," *Phys. Rev.*, vol. 115, no. 1, pp. 2–13, 1959.

[46] J. Kanamori, "Electron correlation and ferromagnetism of transition metals," *Prog. Theor. Phys.*, vol. 30, no. 3, p. 275, 1963.

[47] E. W. Gorter, "Saturation magnetization and crystal chemistry of ferrimagnetic oxides," *Philips Res. Rep.*, vol. 9, pp. 295–320, 1954.

[48] J. M. Hastings and L. M. Corliss, "Neutron diffraction study of manganese ferrite," *Phys. Rev.*, vol. 104, p. 328, 1956.

[49] F. K. Lotgering, "Semiconduction and cation valencies in manganese ferrites," *J. Phys. Chem. Solids*, vol. 25, no. 1, p. 95, Jan. 1964.

[50] D. R. Hartree, "The calculation of atomic structures," *Rep. Prog. Phys.*, vol. 11, p. 113, 1948.

[51] P. Hohenberg and W. Kohn, "Inhomogeneous electron gas," *Phys. Rev.*, vol. 136, no. 3B, p. B864, 1964.

[52] A. Zunger, J. P. Perdew, and G. L. Oliver, "A self-interaction corrected approach to many-electron systems: Beyond the local spin density approximation," *Solid State Commun.*, vol. 34, no. 12, p. 933, Jun. 1980.

[53] J. P. Perdew and Y. Wang, "Accurate and simple density functional for the electronic exchange energy: Generalized gradient approximation," *Phys. Rev. B*, vol. b33, no. 12, p. 8800, Jun. 1986.

[54] A. D. Becke, "Density-functional thermochemistry. I. The effect of the exchange-only gradient correction," *J. Chem. Phys.*, vol. 96, p. 2155, 1992.

[55] V. I. Anisimov, J. Zaanen, and O. K. Anderson, "Band theory and Mott insulators: Hubbard U instead of Stoner I," *Phys. Rev. B*, vol. 44, no. 3, pp. 943–954, 1991.

[56] P. Wei and Z. Q. Qi, "Insulating gap in the transition-metal oxides: A calculation using the local-spin-density approximation with the on-site Coulomb U correlation correction," *Phys. Rev. B*, vol. 49, no. 16, p. 10864, Apr. 1994.

[57] A. D. Becke, "Density-functional thermochemistry. III. The role of exact exchange," *J. Chem. Phys.*, vol. 98, no. 7, p. 5648, 1993.

[58] X. Zuo and C. Vittoria, "Calculation of exchange integrals and electronic structure for manganese ferrite," *Phys. Rev.*, vol. 66, no. 18, p. 184420, Nov. 2002.

[59] A. J. Heager and T. W. Houston, "Nuclear magnetic resonance in ferrimagnetic $MnFe_2O_4$," *Phys. Rev.*, vol. 135, no. 3A, p. A661, 1964.

[60] W. Wegener, D. Scheerlinck, E. Legrand, and S. Hautecler, "Inelastic neutron scattering study of acoustical magnons in $MnFe_2O_4$," *Solid State Commun.*, vol. 15, no. 2, p. 345, Jul. 1974.

[61] D. J. Singh, M. Gupta, and R. Gupta, "First-principles investigation of $MnFe_2O_4$," *Phys. Rev. B*, vol. 65, no. 6, p. 064432-1, 2002.

[62] G. P. Rodrigue, "A generation of microwave ferrite devices," *Proc. IEEE*, vol. 76, no. 2, pp. 121–137, Feb. 1988.

[63] B. Lax, "Frequency and loss characteristics of microwave ferrite devices," *Proc. IRE*, vol. 44, pp. 1368–1386, Oct. 1956.

[64] F. Bertaut and R. Pauthenet, "Crystalline structure and magnetic properties of ferrites having the general formula $5Fe_2O_3.3M_2O_3$," *Proc. Inst. Elec. Eng.*, vol. 104B, pp. 261–264, 1957.

[65] D. J. DeBitetto, F. K. DePre, and F. G. Brockman, "Highly anistropic materials for millimeter wave applications," in *Proc. Symp. Millimeter Waves*, 1959, vol. 9, p. 95.

[66] Y. Chen, A. L. Geiler, T. Sakai, and S. D. Yoon *et al.*, "Microwave and magnetic properties of self-biased barium hexaferrite screen printed thick films," *J. Appl. Phys.*, vol. 99, no. 8, p. 08M904, 2006.
[67] X. Sui, M. Scherge, M. H. Kryder, and J. E. Snyder *et al.*, "Barium ferrite thin-film recording media," *J. Magn. Magn. Mater.*, vol. 155, no. 1–3, pp. 132–139, Mar. 1996.
[68] L. Zhang, X. D. Su, Y. Chen, and Q. F. Li *et al.*, "Radio-frequency magnetron sputter-deposited barium hexaferrite films on pt-coated Si substrates suitable for microwave applications," *Scripta Mater.*, vol. 63, pp. 492–495, 2010.
[69] K. Tanaka, Y. Omata, and Y. Nishikawa *et al.*, "Formation of Ni-Zn-ferrite films using laser ablation," *IEEE Trans. J. Magn. Jpn.*, vol. 6, no. 11, pp. 1001–1006, Nov. 1991.
[70] C. Vittoria, "Fabrication of Ferrite Films Using Laser Deposition," U.S. Patent 5,227,204, 1993, (disclosed 1991).
[71] J. D. Adam, L. E. Davis, G. F. Dionne, E. F. Shloemann, and S. N. Stitzer, "Ferrite devices and materials," *IEEE Trans. Microw. Theory Tech.*, vol. 50, no. 3, pp. 721–737, Mar. 2002.
[72] E. F. Schloemann, "Circulators for microwave and millimeter-wave integrated circuits," *Proc. IEEE*, vol. 76, no. 2, pp. 188–200, Feb. 1988.
[73] A. J. Fenn, D. H. Temme, and W. P. Delaney *et al.*, "The development of phased-array radar development," *Lincoln Lab. J.*, vol. 12, p. 321, 2000.
[74] T. Schaug-Pettersen, Norwegian Electronic Research, ONR Tech. Rep. (BR) ONRL, 1957, vol. 111, p. 57.
[75] L. Davis, J. U. Milano, and J. Saunders, "A strip-line l-band compact circulator," *Proc. IRE*, vol. 48, p. 115, 1960.
[76] B. Hershenov, "All garnet microstrip circulators for integrated circuits," in *IEEE-1967 G-MTT Int. Microwave Symp. Dig.*, May 1967, pp. 142–144.
[77] H. Bosma, "On the principle of stripline circulation," *Proc. IEE*, vol. 109, p. 137, 1962.
[78] H. Bosma, "On stripline Y-circulation at UHF," *IRE Trans. Microw. Theory Tech.*, vol. 12, no. 1, pp. 61–72, Jan. 1964.
[79] C. E. Fay and R. L. Comstock, "Operation of the ferrite junction circulator," *IEEE Trans. Microw. Theory Tech.*, vol. 13, no. 1, pp. 15–27, Jan. 1965.
[80] D. Polder, "On the phenomenology of ferromagnetic resonance," *Phys. Rev.*, vol. 73, no. 9, p. 1120, 1948.
[81] D. Polder, "On the theory of ferromagnetic resonance," *Phil. Mag.*, vol. 40, no. 2, pp. 99–115, 1949.
[82] Y. S. Wu and F. J. Rosenbaum, "Wideband operation of microstrip circulators," *IEEE Trans. Microw. Theory Tech.*, vol. 22, p. 849, 1974.
[83] R. H. Knerr, "An annotated bibliography of microwave circulators and isolators—1968–1975," *IEEE Trans. Microw. Theory Tech.*, vol. MTT-23, pp. 818–825, Oct. 1975.
[84] W. H. von Aulock and C. E. Fay, *Linear Ferrite Devices for Microwave Applications*. New York: Academic Press, 1968.
[85] J. Helszajn, *Nonreciprocal Microwave Junctions and Circulators*. New York: Wiley, 1975.
[86] C. Kittel, "On the theory of ferromagnetic resonance absorption," *Phys. Rev.*, vol. 73, no. 2, p. 155, 1948.
[87] V. G. Harris, A. Geiler, Y. Chen, and S. D. Yoon *et al.*, "Recent advances in processing and applications of microwave ferrites," *J. Magn. Magn. Mater.*, vol. 321, no. 14, pp. 2035–2047, Jul. 2009.
[88] Y. Akaiwa and T. Okazaki, "An application of a hexagonal ferrite to a millimeter-wave Y circulator," *IEEE Trans Magn.*, vol. 10, no. 2, pp. 374–378, Jun. 1974.
[89] J. A. Weiss, N. G. Watson, and G. F. Dionne, "New uniaxial-ferrite millimeter-wave junction circulators," in *IEEE MTT-S Dig.*, Jun. 1989, vol. 1, p. 145.
[90] N. Zeina, H. How, and C. Vittoria, "Self-biasing circulators operating at K_a-band utilizing M-type hexagonal ferrites," *IEEE Trans. Magn.*, vol. 28, no. 5, p. 3219, Sep. 1992.
[91] S. A. Oliver, P. Shi, and W. Hu *et al.*, "Integrated self-biased hexaferrite microstrip circulators for millimeter-wavelength applications," *IEEE Trans. Microw. Theory Tech.*, vol. 49, no. 2, p. 385, Feb. 2001.
[92] P. Shi, S. D. Yoon, X. Zuo, and I. Kozulin *et al.*, "Microwave properties of pulsed laser deposited Sc-doped barium hexaferrite films," *J. Appl. Phys.*, vol. 87, no. 9, p. 4981, 2000.
[93] P. Shi, H. How, and X. Zuo *et al.*, "MMIC circulators using hexaferrites," *IEEE Trans. Magn.*, vol. 37, no. 4, p. 2389, Jul. 2001.
[94] J. W. Wang, A. L. Geiler, V. G. Harris, and C. Vittoria, "Self biased Y-junction circulator at Ku band," *IEEE Microw. Wireless Compon. Lett.*, vol. 21, pp. 292–294, 2011.
[95] L. E. Davis and D. Sillars, "Millimetric nonreciprocal coupled-slot finline components," *IEEE Trans. Microw. Theory Tech.*, vol. 34, no. 7, pp. 804–808, Jul. 1986.
[96] D. Marcuse, "Coupled-mode theory for anisotropic optical waveguides," *Bell Syst. Tech. J.*, vol. 54, no. 6, p. 985, 1975.
[97] C. K. Queck and L. E. Davis, "Microstrip and stripline ferrite-coupled-line (FCL) circulator's," *IEEE Trans. Microw. Theory Tech.*, vol. 50, no. 12, p. 2910, Dec. 2002.
[98] C. K. Queck and L. E. Davis, "Self-biased hexagonal ferrite coupled line circulators," *Electron. Lett.*, vol. 39, no. 22, p. 1595, Oct. 2003.
[99] R. R. Romnanofsky, "Array phase shifters: Theory and technology," in *Antenna Engineering Handbook*. New York: McGraw Hill, 2007, ch. 21, p. 23.
[100] M. I. Bichurin, D. Viehland, and G. Srinivasan, "Magnetoelectric interactions in ferromagnetic-piezoelectric layered structures: Phenomena and devices," *J. Electroceram.*, vol. 19, no. 4, pp. 243–250, 2007.
[101] C. W. Nan, M. I. Bichurin, S. Dong, and D. Viehland, "Multiferroic magnetoelectric composites: Historical perspective, status, and future directions," *J. Appl. Phys.*, vol. 103, no. 3, p. 031101, 2008.
[102] W. Eerenstein, N. D. Mathur, and J. F. Scott, "Multiferroic and magnetoelectric materials," *Nature*, vol. 442, p. 759, Aug. 2006.
[103] Y. K. Fetisov and G. Srinivasan, "Electric field tuning characteristics of a ferrite—Piezoelelectric microwave resonator," *Appl. Phys. Lett.*, vol. 88, p. 143505, 2006.
[104] Y. Chen, T. Fitchorov, C. Vittoria, and V. G. Harris, "Electrically controlled magnetization switching in a multiferroic heterostructure," *Appl. Phys. Lett.*, vol. 97, p. 052502, 2010.
[105] S. Dong, J. Zhai, J. Li, and D. Viehland, "Near-ideal magnetoelectricity in high-permeability magnetostrictive/piezofiber laminates with a (2-1) connectivity," *Appl. Phys. Lett.*, vol. 89, no. 25, p. 252904, 2006.
[106] A. L. Geiler, S. M. Gillette, Y. Chen, and J. Wang *et al.*, "Multiferroic heterostructure fringe field tuning of meander line microstrip ferrite phase shifter," *Appl. Phys. Lett.*, vol. 96, no. 5, p. 053508, 2010.
[107] A. S. Tatarenko, G. Srinivasan, and M. I. Bichurin, "Magnetoelectric microwave phase shifter," *Appl. Phys. Lett.*, vol. 88, no. 18, p. 183507, 2006.
[108] D. R. Smith, J. B. Pendry, and M. C. K. Wiltshire, "Metamaterials and negative refractive index," *Science*, vol. 305, pp. 788–792, 2004.
[109] Y. He, P. He, V. G. Harris, and C. Vittoria, "Role of ferrites in negative index materials," *IEEE Trans. Magn.*, vol. 42, no. 10, pp. 2852–2854, Oct. 2006.
[110] Y. He, P. He, S. D. Yoon, P. V. Parimi, F. J. Rachford, V. G. Harris, and C. Vittoria, "Tunable negative index metamaterial using yttrium iron garnet," *J. Magn. Magn. Mater.*, vol. 313, no. 1, pp. 187–191, 2007.
[111] P. He, P. Parimi, V. G. Harris, and C. Vittoria, "Tunable negative refractive index metamaterials phase shifter," *Electron. Lett.*, vol. 43, no. 25, pp. 1440–1441, Dec. 2007.
[112] P. He, J. Gao, C. Marinis, and P. V. Parimi *et al.*, "A microstrip tunable negative refractive index metamaterial and phase shifter," *Appl. Phys. Lett.*, vol. 93, no. 19, p. 193505, 2008.
[113] P. He, J. Gao, Y. Chen, and P. Parimi *et al.*, "Q-band tunable negative refractive index metamaterials using Sc-doped BaM hexaferrite," *J. Phys. D: Appl. Phys.*, vol. 42, p. 155005, 2009.
[114] R. Levy and S. B. Cohn, "A history of microwave filter research, design, and development," *IEEE Trans. Microw. Theory Tech.*, vol. 32, pp. 1055–1067, Sep. 1984.
[115] J. Uher and W. J. R. Hoefer, "Tunable microwave and millimeter-wave band-pass filters," *IEEE Trans. Microw. Theory Tech.*, vol. 39, no. 4, pp. 643–653, Apr. 1991.
[116] S. Gillette, A. L. Geiler, and Z. Chen *et al.*, "Active tuning of a microstrip hairpin-line microwave bandpass filter on a polycrystalline YIG substrate using small magnetic fields," *J. Appl. Phys.*, vol. 109, p. 07A513, 2011.
[117] A. S. Tatarenko, V. Gheevarughese, and G. Srinivasan, "Magnetoelectric microwave bandpass filter," *Electron. Lett.*, p. 20060167, 2006.
[118] A. V. Mijiritskii and D. O. Boerma, "(0 0 1) surface and morphology of thin Fe_3O_4 layers grown by O_2-assisted molecular beam epitaxy," *Surf. Sci.*, vol. 486, no. 1–2, pp. 73–81, Jul. 2001.
[119] L. Horng, G. Chern, M. C. Chen, P. C. Kang, and D. S. Lee, "Magnetic anisotropic properties in Fe_3O_4 and $CoFe_2O_4$ ferrite epitaxy thin films," *J. Magn. Magn. Mater.*, vol. 270, no. 3, pp. 389–396, Apr. 2004.
[120] S. van Dijken, X. Fain, S. M. Watts, K. Nakajima, and J. M. D. Coey, "Magnetoresistance of Fe_3O_4/Au/Fe_3O_4 and Fe_3O_4/Au/Fe spin-valve structures," *J. Magn. Magn. Mater.*, vol. 280, no. 2–3, pp. 322–326, September 2004.

[121] Z. Cai, T. L. Goodrich, B. Sun, and Z. Chen *et al.*, "Epitaxial growth of barium hexaferrite film on wide bandgap semiconductor 6H-SiC by molecular beam epitaxy," *J. Phys. D.: Appl. Phys.*, vol. 43, p. 095002, 2010.

[122] E. Fujii, H. Torii, A. Tomozawa, R. Takayama, and T. Hiro, "Iron oxide films with spinel, corundum and bixbite structure prepared by plasma-enhanced metalorganic chemical vapor deposition," *J. Cryst. Growth*, vol. 151, no. 1–2, pp. 134–139, May 1995.

[123] E. Fujii and T. Hideo, "Low-temperatures preparation and properties of spinel-type iron oxide films by ECR plasma-enhanced metalorganic chemical vapor deposition," *Jpn. J. Appl. Phys.*, vol. 32, pp. L1527–L1529, 1993.

[124] E. Fujii, H. Torii, and M. Aoki, "Preparation of spinel ferrite thin films by plasma assisted MO-CVD," *IEEE Trans. J. Magn. Jpn.*, vol. 4, no. 8, pp. 512–517, Jul. 1989.

[125] A. Tomozawa, E. Fjuii, H. Torii, and M. Hattori, "Rapid preparation of ferrite films by plasma-enhanced MOCVD," *IEEE Trans. J. Magn. Jpn.*, vol. 9, no. 1, pp. 146–151, Jan.–Feb. 1994.

[126] S. Pignard, J. P. Senateur, H. Vincent, J. Kreisel, and A. Abrutis, "Deposition of $BaFe_{12}O_{19}$ thin films by a new injection-CVD method," *J. Phys. IV France*, vol. 7, pp. C1-483–C1-484, Mar. 1997.

[127] J. E. Snyder, V. G. Harris, N. C. Koon, X. Sui, and M. H. Kryder, "Local structure of the amorphous precursor to Ba-hexaferrite thin films: An anisotropic octahedral Fe-O glass network," *Phys. Rev. Lett.*, vol. 77, no. 16, p. 3383, Oct. 1996.

[128] J. E. Snyder, V. G. Harris, N. C. Koon, X. Sui, and M. H. Kryder, "Determination of local order in the amorphous precursor to Ba-hexaferrite thin-film recording media," *J. Appl. Phys.*, vol. 79, no. 8, pp. 4890–4892, Apr. 1996.

[129] P. R. Dorsey, R. Seed, and C. Vittoria *et al.*, "Oriented barium hexaferrite thin films prepared by pulsed laser deposition," *IEEE Trans., Magn.*, vol. 28, no. 5, pp. 3216–3218, Sep. 1992.

[130] B. M. Simion, R. Ramesh, V. G. Keramidas, G. Thomas, E. Marinero, and R. L. Pfeffer, "Magnetic characterization of epitaxial Y5Fe3012/Eu1Bi2Fe5012 heterostructures grown by pulsed laser deposition," *J. Appl. Phys.*, vol. 76, no. 10, pp. 6287–6289, 1994.

[131] H. Buhay, J. D. Adam, M. R. Daniel, and N. J. Doyle *et al.*, "Thick yttrium-iron-garnet (YIG) films produced by pulsed laser deposition (PLD) for integration applications," *IEEE Trans. Magn.*, vol. 31, no. 6, pp. 3832–3834, Nov. 1995.

[132] Y. Nakata, Y. Tashiro, and T. Okada *et al.*, "Fabrication of Ce:YIG film for electric and magnetic field sensor by pulsed-laser deposition and laser-induced forward transfer," *Proc. SPIE*, vol. 4088, p. 333, 2000.

[133] H. Hayashi, S. Iwasa, and N. J. Vasa *et al.*, "Fabrication of Bi-doped YIG optical thin film for electric current sensor by pulsed laser deposition," *Appl. Surf. Sci.*, vol. 197, p. 463, 2002.

[134] H. Hayashi, S. Iwasa, and N. J. Vasa *et al.*, "Characteristics of Bi:YIG magneto-optic thin films fabricated by pulsed laser deposition method for an optical current transformer," *Jpn. J. Appl. Phys.*, vol. 41, p. 410, 2002.

[135] M. Y. Chern, W. S. Lee, and D. R. Liou, "Curie temperatures of $Y_3Fe_5O_{12}/Gd_3Fe_5O_{12}$ superlattices," *J. Magn. Magn. Mater.*, vol. 170, p. L243, 1997.

[136] Y. Song, S. Kalarickal, and C. E. Patton, "Optimized pulsed laser deposited barium ferrite thin films with narrow ferromagnetic resonance linewidths," *J. Appl. Phys.*, vol. 94, p. 5103, 2003.

[137] R. Welch, T. Jackson, and S. Palmer, "Barium hexaferrite films prepared by pulsed laser deposition," *IEEE Trans. Magn.*, vol. 31, no. 6, pp. 2752–2754, Nov. 1995.

[138] S. D. Yoon, C. Vittoria, and S. A. Oliver, "Magnetization behavior of scandium-substituted barium hexaferrite films having uniaxial axis in the film plane," *J. Magn. Magn. Mater.*, vol. 265, no. 2, p. 130, Sep. 2003.

[139] M. T. Johnson, P. G. Kotula, and J. Carter, "Growth of nickel ferrite thin films using pulsed-laser deposition," *J. Cryst. Growth*, vol. 206, no. 4, p. 299, Nov. 1999.

[140] C. N. Chinnasamy, S. D. Yoon, and A. Yang *et al.*, "Effect of growth temperature on the magnetic, microwave, and cation inversion properties on $NiFe_2O_4$ thin films deposited by pulsed laser ablation deposition," *J. Appl. Phys.*, vol. 101, no. 9, p. 09M517, 2007.

[141] G. Balestrino, S. Martelluci, A. Paoletti, and P. Paroli *et al.*, "Lithium ferrite epitaxial films grown by pulsed laser deposition: Structural and electrical transport properties," *Solid State Commun.*, vol. 96, no. 12, pp. 997–1002, Dec. 1995.

[142] J. F. M. Cillessen, R. M. Wolf, and J. B. Giesbers *et al.*, "Growth, structuring and characterization of all-oxide thin film devices prepared by pulsed laser deposition," *Appl. Surf. Sci.*, vol. 96–98, pp. 744–751, Apr. 1996.

[143] M. Guyot, A. Lisfi, and R. Krishnan *et al.*, "Ferrimagnetic thin films prepared by pulsed laser deposition," *Appl. Suf. Sci.*, vol. 96–98, p. 802, 1996.

[144] M. C. Terzzoli, S. Duhalded, S. Jacobo, L. Steren, and C. Moina, "High perpendicular coercive field of $CoFe_2O_4$ thin films deposited by PLD," *J. Alloys Comp.*, vol. 369, no. 1–2, pp. 209–212, Apr. 2004.

[145] J. A. Paulson, A. P. Ring, C. C. H. Lo, J. E. Snyder, and D. C. Jiles, "Manganese-substituted cobalt ferrite magnetostrictive materials for magnetic stress sensor applications," *J. Appl. Phys.*, vol. 97, p. 044502, 2005.

[146] G. Hu, J. H. Choi, C. B. Eom, V. G. Harris, and Y. Suzuki, "Structural tuning of the magnetic behavior in spinel-structure, ferrite thin films," *Phys. Rev. B*, vol. 62, no. 2, pp. R779–R782, Jul. 2000.

[147] G. Hu, V. G. Harris, and Y. Suzuki, "Microstructure and magnetic properties of cobalt ferrite thin films," *IEEE Trans. Magn.*, vol. 37, no. 4, pp. 2347–2349, Jul. 2001.

[148] A. Yang, Z. Chen, and X. Zuo *et al.*, "Cation-disorder-enhanced magnetization in pulsed-laser-deposited CuFe204 films," *Appl. Phys. Lett.*, vol. 86, p. 252510, 2005.

[149] A. Yang, Z. Chen, S. M. Islam, C. Vittoria, and V. G. Harris, "Cation engineering of Cu-ferrite films deposited by alternating target laser ablation deposition," *J. Appl. Phys.*, vol. 103, no. 7, pp. 07E509-1–07E509-3, Apr. 2008.

[150] X. H. Liu, M. H. Hong, and W. D. Song *et al.*, "Barium ferrite $(BaFe_{12}O_{19})$ thin films prepared by pulsed laser deposition on MgO buffered Si substrates," *Appl. Phys. A*, vol. 80, no. 3, pp. 611–614, 2005.

[151] Y. Chen, I. C. Smith, A. L. Geiler, and C. Vittoria *et al.*, "Microstructural, magnetic and microwave properties of large area $BaFe_{12}O_{19}$ thick films ($> 100\ \mu m$) deposited on $\alpha - SiO_2/Si$ and $\alpha - Al_2O_3/Si$ substrates," *IEEE Trans. Magn.*, vol. 44, no. 12, pp. 4571–4577, 2008.

[152] Y. Chen, I. C. Smith, I. , A. L. Geiler, and C. Vittoria *et al.*, "Realization of hexagonal barium ferrite thick films on Si substrates using a screen printing technique," *J. Phys. D: Appl. Phys.*, vol. 41, p. 095006, 2008.

[153] Z. H. Chen, A. Yang, and Z. H. Cai *et al.*, "Structure and magnetism of Ba-hexaferrite films grown on single crystal 6-H SiC with graduated interfacial MgO buffer layers," *IEEE Trans. Magn.*, vol. 42, no. 10, pp. 2855–2857, Oct. 2006.

[154] Z. H. Chen, A. Yang, S. D. Yoon, and K. Ziemer *et al.*, "Growth of Ba-hexaferrite films on single crystal 6-H SiC," *J. Magn. Magn., Mater.*, vol. 301, no. 1, pp. 166–170, Jun. 2006.

[155] Z. H. Chen, A. Yang, A. L. Geiler, and V. G. Harris *et al.*, "Epitaxial growth of M-type Ba-hexaferrite films on MgO (111)\\SiC (0001) with low ferromagnetic resonance linewidths," *Appl. Phys. Lett.*, vol. 91, no. 18, p. 182505, 2007.

[156] M. Koleva, S. Zotova, and P. Atanasov *et al.*, "Sr-ferrite thin films grown on sapphire by pulsed laser deposition," *Appl. Surf. Sci.*, vol. 168, no. 1–4, p. 108, Dec. 2000.

[157] S. A. Oliver, M. Chen, M. , and C. Vittoria *et al.*, "Properties of pulsed laser deposited scandium-doped barium hexaferrite films," *J. Appl. Phys.*, vol. 85, p. 4630, 1999.

[158] R. Atkinson, P. Papakonstantinou, I. Salter, and R. Gerber, "Optical and magneto-optical properties of Co-Ti-substituted barium hexaferrite single crystals and thin films produced by laser ablation," *J. Magn. Magn. Mater.*, vol. 138, no. 102, pp. 222–231, Nov. 1994.

[159] X. Zuo, A. Yang, R. Mafhoum, and R. Karim *et al.*, "Manganese ferrite grown at the atomic scale," *IEEE Trans. Magn.*, vol. 40, no. 4, pp. 2811–2813, Jul. 2004.

[160] X. Zuo, A. Yang, and S. D. Yoon *et al.*, "Large induced magnetic anisotropy in manganese spinel ferrite films," *Appl. Phys. Lett.*, vol. 87, no. 15, pp. 152505-1–15205-3, Oct. 2005.

[161] X. Zuo, A. Yang, and S. D. Yoon *et al.*, "Magnetic properties of manganese ferrite films grown at atomic scale," *J. Appl. Phys.*, vol. 97, no. 10, p. 10G103, 2005.

[162] A. L. Geiler, Y. He, S. D. Yoon, and A. Yang *et al.*, "Epitaxial growth of $PbFe_{12}O_{19}$ thin films by alternating target laser ablation deposition of Fe_2O_3 and PbO," *J. Appl. Phys.*, vol. 101, no. 9, p. 09M510, 2007.

[163] X. Zuo, A. Yang, C. Vittoria, and V. G. Harris, "Computational study of copper ferrite $(CuFe_2O_4)$," *J. Appl. Phys.*, vol. 99, no. 8, p. 08M909, 2006.

[164] A. L. Geiler, A. Yang, X. Zuo, S. D. Yoon, Y. Chen, V. G. Harris, and C. Vittoria, "Atomic scale design and control of cation distribution in hexagonal ferrites," *Phys. Rev. Lett.*, vol. 101, p. 067201, 2008.

[165] V. G. Harris, N. C. Koon, C. M. Williams, and Q. Zhang *et al.*, "Direct measurement of octahedral and tetrahedral site environments in NiZn-ferrites," *IEEE Trans. Magn*, vol. 31, no. 6, pp. 3473–3475, Nov. 1995.

[166] V. G. Harris, N. C. Koon, C. M. Williams, Q. Zhang, M. Abe, and J. Kirkland, "Cation distributions in spinel ferrites via EXAFS," *Appl. Phys. Lett.*, vol. 68, p. 2082, 1996.
[167] V. G. Harris, C. M. Williams, M. Abe, and Q. Zhang, "Multiple-scattering extended X-ray absorption fine structure analysis of spinel ferrites: Cation site distribution in NiZn-ferrite films," *Le Journal de Physique*, vol. 07, pp. C1-215–C1-218, 1997.
[168] S. Calvin, E. E. Carpenter, V. G. Harris, and S. A. Morrison, "Use of multiple-edge refinement of extended x-ray absorption fine structure to determine site occupancy in mixed ferrite nanoparticles," *Appl. Phys. Lett.*, vol. 81, no. 20, p. 3828, 2002.
[169] A. Yang, Y. Chen, Z. Chen, C. Vittoria, and V. G. Harris, "Magnetic and atomic structure parameters of Sc-doped barium hexagonal ferrites," *J. Appl. Phys.*, vol. 103, p. 07E511, Apr. 2008.
[170] S. Li, V. T. John, C. O'Connor, V. Harris, and E. Carpenter, "Cobalt-ferrite, nanoparticles: Structure, cation distributions, and magnetic properties," *J. Appl. Phys.*, vol. 87, no. 9, p. 6233, 2000.
[171] A. Yang, C. N. Chinnasamy, J. M. Greneche, and Y. Chen *et al.*, "Large tenability of Néel temperature by growth-rate-induced cation inversion in Mn-ferrite nanoparticles," *Appl. Phys. Lett.*, vol. 94, no. 11, p. 113109, 2009.
[172] S. Li, L. Liu, V. T. John, C. J. O'Connor, and V. G. Harris, "Co-ferrite nanoparticles: Correlations between synthesis procedures, structural characteristics and magnetic properties," *IEEE Trans. Magn.*, vol. 37, no. 4, pp. 2350–2352, 2001.
[173] M. Abe and Y. Tamaura, "Ferrite plating in aqueous solution: New technique for preparing magnetic thin film," *J. Appl. Phys.*, vol. 55, no. 6, pp. 2614–2616, Mar. 1984.
[174] M. Abe, "Ferrite plating: A chemical method preparing oxide magnetic films at 24–100 °, and its applications," *Electrochimica Acta*, vol. 45, no. 20, pp. 3337–3343, Jun. 2000.
[175] K. Kondo, Y. Numata, T. Chiba, and S. Yamada *et al.*, "Spin-sprayed ferrite films highly permeable in the GHz range, with excellent heat resistance," *Trans. Magn. Soc.*, vol. 5, no. 4, p. 161, 2005.
[176] M. Abe, Y. Tamaura, Y. Goto, N. Kitamura, and M. Gomi, "High speed deposition of high-quality ferrite films from aqueous solution at low temperatures ($\leq 90°\mathrm{C}$)," *J. Appl. Phys.*, vol. 61, no. 8, pp. 3211–3213, Apr. 1987.
[177] K. Kondo, T. Chiba, H. Ono, and S. Yoshida *et al.*, "Conducted noise suppression up to GHz range by spin-sprayed $Ni_{0.2}Zn_xFe_{2.8-x}O_44$ ($x = 0.3, 0.6$) films having different natural resonance frequencies," *J. Magn. Magn. Mater.*, vol. 301, pp. 107–111, 2006.
[178] K. Kondo, T. Chiba, H. Ono, and S. Yoshida *et al.*, "Conducted noise suppression effect up to 3 GHz by NiZn ferrite film plated at 90 °C directly onto printed circuit board," *J. Appl. Phys.*, vol. 93, no. 10, p. 7130, May 2003.
[179] N. Matsushita, H. Kondo, S. Yoshida, and M. Tada *et al.*, "Ni-Zn ferrite films synthesized from aqueous solution usable for sheet-type conducted noise suppressors in GHz range," *J. Electroceram.*, vol. 16, no. 4, p. 557, 2006.
[180] K. Kondo, S. Yoshida, H. Ono, and M. Abe, "Spin sprayed Ni(-Zn)-Co ferrite films with natural resonance frequency exceeding 3 GHz," *J. Appl. Phys.*, vol. 101, no. 9, p. 09M502, 2007.
[181] R. C. Linares, "Epitaxial growth of narrow linewidth yttrium iron garnet films," *J. Cryst. Growth*, vol. 3–4, pp. 443–446, 1968.
[182] T. Hibiya, "Surface morphologies and quality of thick liquid phase epitaxial garnet films for magneto-optic devices," *J. Cryst. Growth*, vol. 62, no. 1, p. 87, Jun. 1983.
[183] H. L. Glass, "Ferrite films for microwave and millimeter-wave devices," *Proc. IEEE*, vol. 76, no. 2, p. 151, Feb. 1988.
[184] J. M. Robertson, M. Jansen, B. Hoekstra, and P. F. Bongers, "Growth of spinel ferrite films by liquid phase epitaxy," *J. Cryst. Growth*, vol. 41, no. 1, pp. 29–35, 1977.
[185] F. S. Stearns and H. L. Glass, "Liquid phase epitaxy of hexagonal ferrites and spinel ferrites on non-magnetic spinel substrates," *Mat. Res. Bull.*, vol. 11, no. 10, p. 1319, Oct. 1976.
[186] S. G. Wang, S. D. Yoon, and C. Vittoria, "Microwave and magnetic properties of double-sided hexaferrite films on (111) magnesium oxide substrates," *J. Appl. Phys.*, vol. 92, no. 11, pp. 6728–6732, Jun. 18, 2009.
[187] M. Mita, "Two-magnon ferrimagnetic resonance linewidth of hexagonal ferrite Zn_2Y," *J. Phys. Soc. Jpn.*, vol. 24, pp. 725–728, 1968.
[188] M. Labeyrie, J. S. Mage, and W. Simonet *et al.*, "FMR linewidth of barium hexaferrites at millimeter wavelength," *IEEE Trans. Magn.*, vol. 22, pp. 1224–1226, 1984.
[189] S. D. Yoon and C. Vittoria, "Microwave and magnetic properties of barium hexaferrite films having the c-axis in the film plane by liquid phase epitaxy technique," *J. Appl. Phys.*, vol. 93, p. 8597, 2003.
[190] S. D. Yoon and C. Vittoria, "Thick M-type barium hexaferrite films grown on garnet substrates," *J. Appl. Phys.*, vol. 96, p. 2131, 2004.
[191] S. D. Yoon and C. Vittoria, "Preparation of high-quality hexaferrite thick films by an improved liquid phase epitaxy deposition technique," *IEEE Trans. Magn.*, vol. 39, no. 5, pp. 3163–3165, Sep. 2003.
[192] J. Topfer, J. Murbe, A. Angermann, and S. Kracunovska *et al.*, "Soft ferrite materials for ultilayer inductors," *Int. J. Appl. Ceram. Technol.*, vol. 3, no. 6, p. 455, Nov. 2006.
[193] V. G. Harris, Z. Chen, Y. Chen, and S. Yoon *et al.*, "Ba-hexaferrite films for next generation microwave devices," *J. Appl. Phys.*, vol. 99, no. 8, p. 08M911, 2006.
[194] Z. C. Yuan, A. J. Williams, T. C. Shields, S. Blackburn, and C. B. Ponton, "The production of Sr hexaferrite thick films by screen printing," *J. Magn. Magn. Mater.*, vol. 247, no. 3, p. 257, Jun. 2002.
[195] Y. Chen,, T. Sakai, T. Chen, S. D. Yoon, A. L. Geiler, C. Vittoria, and V. G. Harris, "Oriented barium hexaferrite thick films with narrow ferromagnetic resonance linewidth," *Appl. Phys. Lett.*, vol. 88, p. 062516, 2006.
[196] Y. Chen *et al.*, "Screen printed thick self biased, low loss, barium hexaferrite films by hot-press sintering," *J. Appl. Phys.*, vol. 100, p. 043907, 2006.
[197] B. Lax and K. J. Button, *Microwave Ferrites and Ferrimagnetics*. New York: McGraw Hill, 1962.
[198] M. H. Phan, M. B. Morales, C. N. Chinnasamy, and B. Latha *et al.*, "Magnetocaloric effect in bulk and nanostructured $Gd_3Fe_5O_{12}$ materials," *J. Phys. D: Appl. Phys.*, vol. 42, no. 11, p. 115007, Jun. 2009.
[199] S. A. Morrison, C. L. Cahill, E. E. Carpenter, S. Calvin, and V. G. Harris, "Preparation and characterization of MnZn-ferrite nanoparticles using reverse micelles," *J. Appl. Phys.*, vol. 9, no. 10, p. 7489, 2003.
[200] V. G. Harris, D. J. Fatemi, J. O. Cross, and E. E. Carpenter *et al.*, "One-step processing of spinel ferrites via the high-energy ball milling of binary oxides," *J. Appl. Phys.*, vol. 94, no. 1, p. 496, 2003.
[201] D. J. Fatemi, V. G. Harris, M. X. Chen, S. K. Malik, W. B. Yelon, G. J. Long, A. Mohan, and F. Grandjean, "X-ray absorption, neutron diffraction, and Mossbauer spectroscopy studies of MnZn-ferrite processed through high-energy ball-milling," *J. Appl. Phys.*, vol. 85, p. 5172, 1999.
[202] S. Calvin, E. E. Carpenter, B. Ravel, V. G. Harris, and S. A. Morrison, "Use of multiedge refinement of extended x-ray absorption fine structure of manganese zinc ferrite nanoparticles," *Appl. Phys. Lett.*, vol. 81, no. 20, p. 3828, 2002.
[203] S. A. Morrison, C. L. Cahill, E. E. Carpenter, S. Calvin, R. Swaminath, M. E. McHenry, and V. G. Harris, "Magnetic and structural properties of nickel zinc ferrite nanoparticles synthesized at room temperature," *J. Appl. Phys.*, vol. 95, p. 6392, 2004.
[204] S. Calvin, M. M. Miller, R. Goswami, S.-F. Cheng, S. P. Mulvaney, L. J. Whitman, and V. G. Harris, "Determination of crystallite size in a magnetic nanocomposite using extended x-ray absorption fine structure," *J. Appl. Phys.*, vol. 94, p. 778, 2003.
[205] S. Calvin, E. E. Carpenter, B. Ravel, V. G. Harris, and S. A. Morrison, "Multiedge refinement of extended x-ray-absorption fine structure of manganese zinc ferrite nanoparticles," *Phys. Rev.*, vol. B66, p. 224405, 2002.
[206] V. B. Bregar, "Advantages of ferromagnetic nanoparticle composites in microwave absorbers," *IEEE Trans. Magn.*, vol. 40, pp. 1679–1684, May 2004.
[207] Y. Chen, M. J. Nedoroscik, A. L. Geiler, C. Vittoria, and V. G. Harris, "Perpendicularly oriented polycrystalline $BaFe_{11.1}Sc_{0.9}O_{19}$ hexaferrite with narrow FMR linewidth," *J. Amer. Ceram. Soc.*, vol. 91, pp. 2952–2956, 2008.
[208] Y. Chen, T. Fitchorov, A. Koblischka-Veneva, M. R. Koblischka, C. Vittoria, and V. G. Harris, "Topochemical growth of highly textured hexaferrite polycrystalline compacts from oriented antiferromagnetic α-FeOOH nanorods," *Nanotechnology*, vol. 20, p. 445606, 2009.
[209] Y. Chen, A. L. Geiler, T. Chen, T. Sakai, C. Vittoria, and V. G. Harris, "Low-loss barium ferrite quasi-single-crystals for microwave application," *J. Appl. Phys.*, vol. 101, p. 09M501, 2007.
[210] A. Daigle, E. DuPre', A. Geiler, Y. Chen, P. V. Parimi, C. Vittoria, and V. G. Harris, "Preparation and characterization of pure-phase Co2Y ferrite powders via a scalable aqueous coprecipitation method," *J. Amer. Ceram. Soc.*, vol. 93, no. 10, pp. 2994–2997, 2010.
[211] Landolt-Bornstein, "Numerical data and functional relationships in science and technology," in *Magnetic and Other Properties of Oxides and Related Compounds*, K. H. Hellwege and A. M. Hellwege, Eds. Berlin, Germany: Springer, 1970, vol. 4, pt. B, pp. 593–603.

[212] M. Obol and C. Vittoria, "Magnetic properties of Co2Y-type hexaferrite particles oriented in a rotating field," *IEEE Trans. Magn.*, vol. 39, no. 5, pp. 3103–3105, Sep. 2003.
[213] Kato *et al.*, "Performance of Z-type hexagonal ferrite core under demagnetizing and external static fields," *J. Appl. Phys.*, vol. 108, p. 033903, 2010.
[214] J. Smit and H. P. J. Wijn, "Intrinsic properties of ferrites with hexagonal crystal structure," in *Ferrites*. New York: Wiley, 1959, ch. 9, pp. 177–210.
[215] A. P. Daigle, A. L. Geiler, E. Dupré, Y. Chen, P. V. Parimi, C. Vittoria, and V. G. Harris, "Numeric simulations of a novel wideband electromagnetic band gap metamaterial utilizing oriented cobalt-substituted Z-type barium hexaferrites," *IEEE Magn. Lett.*, vol. 2, pp. 0500104–0500104, 2011.
[216] P. Curie, "Sur la symétrie dans les phénomènes physiques," *J. Phys. 3e Series*, vol. 3, p. 393, 1894.
[217] I. E. Dzyaloshinskii, "On the magneto-electrical effect in antiferromagnets," *Sov. Phys. JETP*, vol. 10, p. 628, 1960.
[218] D. N. Astrov, "The magnetoelectric effect in antiferromagnetics," *Sov. Phys. JETP*, vol. 11, p. 708, 1960.
[219] G. T. Rado, "Observation and possible mechanisms of magnetoelectric effects in a ferromagnet," *Phys. Rev. Lett.*, vol. 13, p. 335, 1964.
[220] T. Kimura, G. Lawes, and A. P. Ramirez, "Ferroelectricity and giant magnetocapacitance in perovskite rare-earth manganites," *Phys. Rev. Lett.*, vol. 94, p. 137201, 2005.
[221] T. Kimura, T. Goto, and H. Shintani *et al.*, "Magnetic control of ferroelectric polarization," *Nature*, vol. 426, p. 55, 2003.
[222] H. Kojima, *Ferromagnetic Materials*, E. P. Wohlfarth, Ed. Amsterdam, The Netherlands: North Holland, vol. 3, p. 305.
[223] S. Ishiwata, Y. Taguchi, and H. Murakawa *et al.*, "Low-magnetic-field control of electric polarization vector in a helimagnet," *Science*, vol. 319, p. 1643, 2008.
[224] Y. Kitagawa, Y. Hiraoka, and T. Honda *et al.*, "Low-field magnetoelectric effect at room temperature," *Nature Mater.*, vol. 9, p. 797, 2010.
[225] L. O. Chua, "Memristor-the missing circuit element," *IEEE Trans. Circuit Theory*, vol. 18, pp. 507–519, 1971.
[226] D. B. Strukov, G. S. Snider, D. R. Stewart, and R. S. Williams, "The missing memristor found," *Nature*, vol. 453, pp. 80–83, 2008.
[227] J. J. Yang, M. D. Pickett, and X. Li *et al.*, "Memristive switching mechanisms for metal/oxide/metal nanodevices," *Nature Nanotechnol.*, vol. 3, pp. 429–433, 2008.
[228] T. H. Kim, E. Y. Jang, and N. J. Lee *et al.*, "Nanoparticle assemblies as memristors," *Nano Lett.*, vol. 9, pp. 2229–2233, 2009.
[229] K. Cai, R. Wang, B. Li, and J. Zhou, "Hysteresis current-voltage characteristics in polycrystalline ceramic ferrites," *Appl. Phys. Lett.*, vol. 97, p. 122501, 2010.
[230] Y. Chen, X.-Y. Zhang, C. Vittoria, and V. G. Harris, "Giant magnetodielectric effect and magnetic field tunable dielectric resonance in spinel MnZn ferrite," *Appl. Phys. Lett.*, vol. 94, p. 102906, 2009.
[231] M. Wu, B. Kalinikos, and C. E. Patton, "Self generation of chaotic solitary spin wave pulses in magnetic film active feedback rings," *Phys. Rev. Lett.*, vol. 95, p. 237202, 2005.
[232] M. Wu and C. E. Patton, "Experimental observation of fermi-pasta-ulam recurrence in a nonlinear feedback ring system," *Phys. Rev. Lett.*, vol. 98, p. 047202, 2007.

Vincent G. Harris (F'08) has had a distinguished career as an engineer, scientist, inventor, entrepreneur, and leader of engineers and scientists for more than 25 years. He presently holds positions as University Distinguished Professor and William Lincoln Smith Chair Professor of Electrical and Computer Engineering at Northeastern University (NEU). He is the Founder and Director of the Center for Microwave Magnetic Materials and Integrated Circuits ($\mathrm{CM^3IC}$) at NEU whose mission is to develop next generation microwave materials and device solutions for radar and wireless communication technologies for U.S. Defense and commercial industries. From 2008 to 2010, Harris held a guest appointment as Professor of the National Security Institute at the Naval Postgraduate School (Monterey, CA), and from 1990 to 2003, positions as member of the technical staff, Head of the Complex Materials Section, and Head of the Materials Physics Branch at the Naval Research Laboratory (Washington, DC). His research interests include materials design and the study of processing, structure and magnetism in a wide range of electronic materials and devices used principally in microwave applications. He has published more than 275 technical articles in peer-reviewed science and engineering journals, including book reviews and review articles on the topical areas of nanotechnology, magnetism, and microwave materials and devices. In 2007, Harris was named a Distinguished Lecturer by the Institute of Electrical and Electronic Engineering Magnetics Society on the topic of *Frontiers in Ferrite Materials Research and Microwave Device Applications*. Professor Harris is a member of the Editorial Boards of *IEEE Magnetics Letters*, *Advanced Science Letters*, and *Science of Advanced Materials*, he is also the Associate Editor of *SAM*. He is the Founder of Metamagnetics Inc., a for-profit, verteran-owned, small business and serves as Chairman of the Board of Directors.

Prof. Harris is a Fellow of the American Physical Society, the Institute of Physics (Great Britain), and the Institute of Engineering and Technology (Great Britain). He is a veteran of the U.S. Coast Guard.